

Constrained Secrecy Capacity of Finite-Input Intersymbol Interference Wiretap Channels

Aria Nouri, *Student Member, IEEE*, Reza Asvadi, *Senior Member, IEEE*,
Jun Chen, *Senior Member, IEEE*, and Pascal O. Vontobel, *Fellow, IEEE*

Abstract

We consider reliable and secure communication over intersymbol interference wiretap channels (ISI-WTCs). In particular, we first examine the setup where the source at the input of an ISI-WTC is unconstrained and then, based on a general achievability result for arbitrary wiretap channels, we derive an achievable secure information rate for this ISI-WTC. Afterwards, we examine the setup where the source at the input of an ISI-WTC is constrained to be a finite-state machine source (FSMS) of a certain order and structure. Optimizing the parameters of this FSMS toward maximizing the secure information rate is a computationally intractable problem in general, and so, toward finding a local maximum, we propose an iterative algorithm that at every iteration replaces the secure information rate function by a suitable surrogate function whose maximum can be found efficiently. Although the secure information rates achieved in the unconstrained setup are expected to be larger than the secure information rates achieved in the constrained setup, the latter setup has the advantage of leading to efficient algorithms for estimating achievable secure rates and also has the benefit of being the basis of efficient encoding and decoding schemes.

Index Terms

Intersymbol interference (ISI), intersymbol interference wiretap channel (ISI-WTC), finite-state machine channel, finite-state machine source, wiretap channel, secure rate, rate optimization.

A. Nouri and R. Asvadi are with the Cognitive Telecommunication Research Group, Department of Telecommunications, Faculty of Electrical Engineering, Shahid Beheshti University, Tehran, Iran. (e-mails: ar.nouri@mail.sbu.ac.ir; r_asvadi@sbu.ac.ir) R. Asvadi is the corresponding author.

J. Chen is with the Department of Electrical and Computer Engineering, McMaster University, Hamilton, ON, Canada (e-mail: junchen@mail.ece.mcmaster.ca).

P.O. Vontobel is with the Department of Information Engineering and the Institute of Theoretical Computer Science and Communications, The Chinese University of Hong Kong, Hong Kong SAR (e-mail: pascal.vontobel@ieee.org).

I. INTRODUCTION

The increasing number of connected users and the broadcasting nature of the wireless medium lead to a flurry of security challenges for wireless communications applications. For example, typical cryptographic protocols use up communication resources for distributing and maintaining a secret key. This issue significantly decreases the efficiency of the transmission as the number of users exceeds a certain scale [1]. Moreover, traditional cryptosystems rely on the limited eavesdropper's computational power assumption, making them quite vulnerable against the advent of quantum computers [2]. Alternatively, information-theoretic secrecy [3] utilizes the inherent randomness of communication channels (e.g., noise and interference) to achieve security at the physical layer [4], without requiring secret key agreement and without imposing any constraint on the eavesdropper's computational power.

The emergence of different wireless applications gives rise to diverse channel models for various channel conditions. Intersymbol interference (ISI) channels, also known as partial-response channels [5, Ch. 9], are used as a model for high data rate transmission over wireless channels when the symbol duration is much smaller than the delay spread of the channel. This phenomenon in wireless propagation is referred to as frequency-selective multipath fading as well [5]. In order to be specific, let X_t , Y_t , and N_t denote the input, the output, and the additive noise of this channel at the discrete time index t . Moreover, let m be the total number of paths, $g_\ell(t)$ be the gain of the ℓ -th path at time index t , and τ_ℓ be the delay of the ℓ -th path, for all $1 \leq \ell \leq m$. The general model for such a multipath fading is $Y_t \triangleq \sum_{\ell=1}^m g_\ell(t)X_{t-\tau_\ell} + N_t$. This ISI model usually appears in single-carrier communications, where a higher power efficiency and a better peak-to-average power ratio compared with multicarrier modulations are required, e.g., applications of the narrowband internet of things (NB-IoT) [6] as outlined in 5G and beyond networks [7]. Furthermore, the multipath effect also causes ISI in long range underwater acoustic communications [8].

Providing security at the physical layer of the above-mentioned communication setups without imposing extra delay, power consumption, and processing burden, has received significant attention recently [9]–[11]. In this study, we consider the theoretical aspects of physical layer security over ISI channels. In order to focus on the information-conceptual aspects of the memory, channel gains are assumed to be time-invariant, which is a reasonable

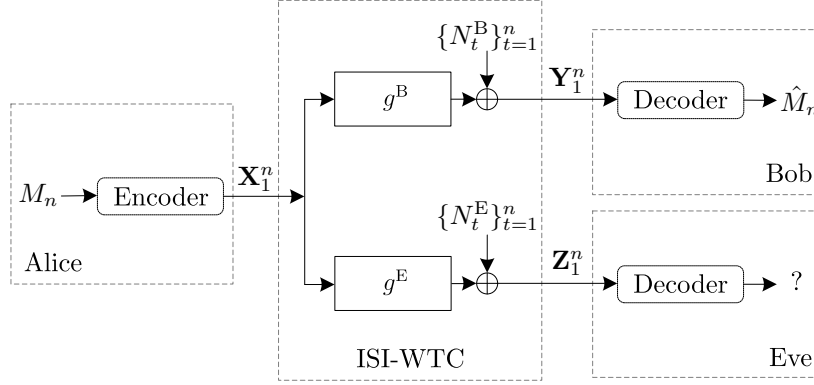


Fig. 1: Block diagram of the ISI-WTC.

assumption in fixed wireless access networks [12], [13]. An intersymbol interference wiretap channel (ISI-WTC) comprises two ISI channels, where the primary channel connects a transmitter (called Alice) to a legitimate receiver (called Bob and abbreviated by “B”), and where the secondary channel connects the transmitter to an eavesdropper (called Eve and abbreviated by “E”), see Fig. 1.

ISI channels with finite input alphabets are a particular case of finite-state machine channels (FSMCs) [14]. Toward maximizing the achievable information rates over FSMCs, the classical Blahut-Arimoto algorithm (BAA) [15], [16] was generalized in [17] to optimize finite-state machine sources (FSMSs) at the input of FSMCs. Comparing the maximized achievable information rates (lower bounds on the capacity) [17], [18] with upper bounds on the capacity [19], [20] of FSMCs, typically shows a small gap between them, which can be further narrowed by increasing the memory order of the employed FSMS at the input [21].

Recently, Han et al. [22], [23] derived the secrecy capacity of memoryless wiretap channels with both causal and non-causal channel state information at the encoder. Dai et al. [24] applied these results to the case of physically degraded Gaussian wiretap channels with a noiseless private feedback from Bob’s observations to the encoder. It is shown in [24] that the considered feedback enhances the secrecy capacity under the weak secrecy criterion. The delayed version of this feedback is employed in [25] to enlarge the rate-equivocation region of finite-state Markov wiretap channels.¹ In addition, enhancing the efficiency of secure

¹In the terminology of [25], Bob’s and Eve’s channels are FSMCs, and the state process is assumed to be a stationary irreducible aperiodic ergodic Markov chain independent of the transmitted messages.

communications over ISI channels by the injection of cooperative artificial noise to mask Eve's observations while minimizing the impact on Bob's channel is studied in [26], [27].

Due to the power efficiency requirements, the artificial noise-aided transmission has not received so much attention in recent standards. Also, establishing a private noiseless channel to feedback the complete output of Bob's channel to Alice's encoder imposes a tremendous delay and processing overload on the higher layers of large cooperative networks. Therefore, we focus on the standard version of the ISI-WTC (with neither feedback nor additional artificial noise) as it requires few assumptions and consequently is more practically relevant.

In terms of the main focus of this paper, estimation of the secrecy capacity of a finite-state wiretap channel is considered in [28]². The problem formulation in [28] resembles the general assumptions of discrete-memoryless wiretap channels [29], where Eve's channel is assumed to be noisier than Bob's channel. However, as we discuss in this paper, these assumptions are invalid for ISI channels (and generally, for FSMCs) due to a non-flat frequency response of these channels. Another issue in [28] corresponds to the employed approximating function for the secure information rate. In particular, the gradient of the approximating function is not the same as the gradient of the secure information rate at a given operating point, which leads to an inaccurate search direction and eventually makes the algorithm unstable.

In the following, we highlight the main contributions and results presented in this study.

- We consider an ISI-WTC where the input symbols are limited to some finite alphabet. In a first step, we study the *unconstrained* setup, i.e., the setup where no constraints are placed on the input distribution. In this setup, the achievable secure information rates are derived under a secrecy criterion that measures the statistical independence between the secret message and Eve's observations using the variational distance.
- Since the optimized Markov sources with a sufficiently large order approach the capacity of FSMCs in a point-to-point setup [17], [21], we then consider the *constrained* setup, i.e., the setup where Alice's source is an FSMS with a given structure (resembles a Markov source of a specific order). Accordingly, we propose an efficient algorithm for optimizing the parameters of this FSMS toward maximizing the achievable secure information rates.

²The finite-state wiretap channel is defined as a wiretap channel where Bob and Eve observe the input source through two distinct FSMCs.

- The above-mentioned secure information rate is not a closed-form function of the input distribution, and its evaluation is only possible through the Monte-Carlo simulations. Hence, the maximization of this function can not be performed by existing numerical methods. The key idea behind the proposed algorithm is to approximate the secure information rate by suitable surrogate functions that are well-defined over a polytope and can relatively easily be maximized. The proposed algorithm resembles the well-known expectation-maximization (EM) algorithm and has a similar convergence behavior.
- We provide examples where the capacity of Eve's channel is higher than the capacity of Bob's channel. These examples exhibit the feasibility of achieving positive secure information rates by exploiting the frequencies where Bob's channel has a higher gain-to-noise spectrum ratio than Eve's channel. In particular, the optimization algorithm tunes the input FSMSs to suitably exploit these discrepancies—without any further power consumption to transmit interfering artificial noise toward jamming Eve's signal.

The remainder of this paper is organized as follows. Section II introduces the system model and some preliminary concepts related to FSMSs, FSMCs, and ISI-WTCs. Section III-A gives a concise discussion about the employed secrecy criterion, based on which Section III-B presents achievability results on the (unconstrained and constrained) secure information rate of ISI-WTCs. Section III-C discusses an efficient algorithm for estimating the secure rate for a given FSMS at the input of an ISI-WTC. Section IV describes the proposed algorithm for optimizing the FSMS at the input of an ISI-WTC and analyzes it in detail. Section V contains some numerical results and discussions. Finally, Section VI draws the conclusion.

A. Notation

The sets of integers and real numbers are denoted by \mathbb{Z} and \mathbb{R} , respectively. Also, the ring of polynomials over \mathbb{R} , with the indeterminate D standing for time delay, is denoted by $\mathbb{R}[D]$. Other than that, sets are denoted by calligraphic letters, e.g., \mathcal{S} . The Cartesian product of two sets \mathcal{X} and \mathcal{Y} is written as $\mathcal{X} \times \mathcal{Y}$, and the n -fold Cartesian product of \mathcal{X} with itself is written as \mathcal{X}^n . If \mathcal{X} is a finite set, then its cardinality is denoted by $|\mathcal{X}|$.

Random variables are denoted by upper-case italic letters, e.g., X , their realizations by the corresponding lower-case letters, e.g., x , and the set of possible values by the corresponding

calligraphic letter, e.g., \mathcal{X} . Random vectors are denoted by upper-case boldface letters, e.g., \mathbf{X} , and their realizations by the corresponding lower-case letters, e.g., \mathbf{x} . For integers n_1 and n_2 satisfying $n_1 \leq n_2$, the notation $\mathbf{X}_{n_1}^{n_2} \triangleq (X_{n_1}, X_{n_1+1}, \dots, X_{n_2})$ is used for a time-indexed vector of random variables and $\mathbf{x}_{n_1}^{n_2} \triangleq (x_{n_1}, x_{n_1+1}, \dots, x_{n_2})$ for its realization.

The probability of an event ξ is denoted by $\Pr(\xi)$. Furthermore, $p_X(\cdot)$ denotes the probability mass function (PMF) of X if X is a discrete random variable and the probability density function (PDF) of X if X is a continuous random variable. Similarly, $p_{Y|X}(\cdot|x)$ denotes the conditional PMF of Y given $X = x$ if Y is a discrete random variable and the conditional PDF of Y given $X = x$ if Y is a continuous random variable.

Note that boldface letters are also used for (deterministic) matrices, e.g., \mathbf{A} , with the (i, j) -entry of \mathbf{A} being called A_{ij} .

Let $\mathbb{1}(\cdot)$ and $\log(\cdot)$ denote the indicator function and the natural logarithm function, respectively. The entropy of a random variable X , the mutual information between two random variables X and Y , and the mutual information between two random variables X and Y conditioned on the random variable Z are denoted by $H(X)$, $I(X; Y)$, and $I(X; Y|Z)$, respectively. The *information density* between the respective realizations of random variables X and Y is defined to be

$$i(x; y) \triangleq \log \left(\frac{p_{X,Y}(x, y)}{p_X(x) \cdot p_Y(y)} \right).$$

Moreover, the *conditional information density* between the respective realizations of random variables X and Y given $Z = z$ is

$$i(x; y|z) \triangleq \log \left(\frac{p_{X,Y|Z}(x, y|z)}{p_{X|Z}(x|z) \cdot p_{Y|Z}(y|z)} \right).$$

Note that

$$I(X; Y) = \sum_{x,y} p_{X,Y}(x, y) \cdot i(x; y), \quad I(X; Y|Z) = \sum_{x,y,z} p_{X,Y,Z}(x, y, z) \cdot i(x; y|z).$$

Finally, the variational distance between the PMFs of two random variables X and Y over the same finite alphabet \mathcal{X} is defined as $d_{\mathcal{X}}(p_X, p_Y) \triangleq \sum_{x \in \mathcal{X}} |p_X(x) - p_Y(x)|$.

II. SYSTEM MODEL

This section gives the definitions of finite-state machine sources (FSMSs) and finite-state machine channels (FSMCs) along with special cases as far as relevant for this study. Based on these definitions, we introduce the finite-state joint source-wiretap channels (FS-JSWTCs), which is the key element for studying FSMSs at the input of ISI-WTCs. The interested reader is referred to [14], [17] for more background and further examples.

Definition 1 (Finite-State Machine Source (FSMS)). A time-invariant (discrete-time) FSMS has a state process $\{\bar{S}_t\}_{t \in \mathbb{Z}}$ and an output process $\{X_t\}_{t \in \mathbb{Z}}$, where $\bar{S}_t \in \bar{\mathcal{S}}$ and $X_t \in \mathcal{X}$ for all $t \in \mathbb{Z}$. We assume that the alphabets $\bar{\mathcal{S}}$ and \mathcal{X} are finite and that for any positive integer n the joint PMF of $\bar{\mathbf{S}}_1^n$ and \mathbf{X}_1^n conditioned on $\bar{S}_0 = \bar{s}_0$ decomposes as

$$p_{\mathbf{X}_1^n, \bar{\mathbf{S}}_1^n | \bar{S}_0}(\mathbf{x}_1^n, \bar{\mathbf{s}}_1^n | \bar{s}_0) = \prod_{t=1}^n p_{X_t, \bar{S}_t | \bar{S}_{t-1}}(x_t, \bar{s}_t | \bar{s}_{t-1}),$$

where $p_{X_t, \bar{S}_t | \bar{S}_{t-1}}(x_t, \bar{s}_t | \bar{s}_{t-1})$ is independent of t . \square

Remark 2. In the following, we will mostly consider FSMSs where $\bar{s}_t \triangleq \mathbf{x}_{t-\bar{\nu}+1}^t$ ($\bar{\mathcal{S}} \triangleq \mathcal{X}^{\bar{\nu}}$) for all $t \in \mathbb{Z}$ and for some positive integer $\bar{\nu}$ (called the memory order of such an FSMS). Considering $\bar{s}_{t-1} = \mathbf{x}_{t-\bar{\nu}}^{t-1}$ and $\bar{s}_t \triangleq \mathbf{x}_{t-\bar{\nu}+1}^t$, it holds that

$$\begin{aligned} p_{X_t, \bar{S}_t | \bar{S}_{t-1}}(x_t, \bar{s}_t | \bar{s}_{t-1}) &= p_{X_t | \bar{S}_{t-1}}(x_t | \bar{s}_{t-1}) \\ &= p_{X_t | X_{t-\bar{\nu}}^{t-1}}(x_t | \mathbf{x}_{t-\bar{\nu}}^{t-1}), \end{aligned}$$

which implies a bijection between the source state sequence and the source output sequence, i.e., the state sequence uniquely determines the output sequence and vice versa. Obviously, such an FSMS is characterized by the triple $(\mathcal{X}, \bar{\nu}, p_{X_t | X_{t-\bar{\nu}}^{t-1}}(x_t | \mathbf{x}_{t-\bar{\nu}}^{t-1}))$. \square

Note that all possible state sequences of an FSMS can be represented by a trellis diagram. Because of the assumed time-invariance, it is sufficient to show a single trellis section. For example, Fig. 2(a) shows a trellis section corresponding to an FSMS characterized by the triple $(\mathcal{X} \triangleq \{+1, -1\}, \bar{\nu} \triangleq 3, p_{X_t | X_{t-3}^{t-1}}(x_t | \mathbf{x}_{t-3}^{t-1}))$.

Before giving the definition of an ISI channel we introduce the more general class of finite-state machine channels (which were called finite-state channels in [14]).

Definition 3 (Finite-State Machine Channel (FSMC)). A time-invariant FSMC has an input process $\{X_t\}_{t \in \mathbb{Z}}$, an output process $\{Y_t\}_{t \in \mathbb{Z}}$, and a state process $\{S'_t\}_{t \in \mathbb{Z}}$, where $X_t \in \mathcal{X}$, $Y_t \in \mathcal{Y}$, and $S'_t \in \mathcal{S}'$ for all $t \in \mathbb{Z}$. We assume that the alphabets \mathcal{X} and \mathcal{S}' are finite and that for any positive integer n the joint PMF/PDF of \mathbf{S}'_1^n and \mathbf{Y}_1^n conditioned on $S'_0 = s'_0$ and $\mathbf{X}_1^n = \mathbf{x}_1^n$ is

$$p_{\mathbf{S}'_1^n, \mathbf{Y}_1^n | S'_0, \mathbf{X}_1^n}(\mathbf{s}'_1^n, \mathbf{y}_1^n | s'_0, \mathbf{x}_1^n) = \prod_{t=1}^n p_{S'_t, Y_t | S'_{t-1}, X_t}(s'_t, y_t | s'_{t-1}, x_t),$$

where $p_{S'_t, Y_t | S'_{t-1}, X_t}(s'_t, y_t | s'_{t-1}, x_t)$ is independent of t . \square

An important special case of an FSMC is an ISI channel.

Definition 4 (Intersymbol Interference (ISI) Channel). An ISI channel with a transfer polynomial $g(D) \triangleq \sum_{t=0}^m g_t D^t \in \mathbb{R}[D]$, where m is called the memory length, has an input process $\{X_t\}_{t \in \mathbb{Z}}$, a noiseless output process $\{U_t\}_{t \in \mathbb{Z}}$, a noise process $\{N_t\}_{t \in \mathbb{Z}}$, and a noisy output process $\{Y_t\}_{t \in \mathbb{Z}}$, where

$$U_t \triangleq \sum_{\ell=0}^m g_\ell X_{t-\ell}, \quad t \in \mathbb{Z},$$

$$Y_t \triangleq U_t + N_t, \quad t \in \mathbb{Z},$$

and where $X_t, U_t, N_t, Y_t \in \mathbb{R}$ for all $t \in \mathbb{Z}$. In the following, we will assume that the noise process is white Gaussian noise, i.e., $\{N_t\}_{t \in \mathbb{Z}}$ are i.i.d. Gaussian random variables with mean zero and variance σ^2 . Clearly, an ISI channel is parameterized by the couple $(g(D), \sigma^2)$. \square

An ISI channel described by the couple $(g(D) \triangleq \sum_{t=0}^m g_t D^t, \sigma^2)$ and having an input process $\{X_t\}_{t \in \mathbb{Z}}$ taking values in a finite set $\mathcal{X} \subsetneq \mathbb{R}$, is a special case of an FSMC. Indeed, let $\mathcal{S}' \triangleq \mathcal{X}^m$. Then

$$p_{S'_t, Y_t | S'_{t-1}, X_t}(s'_t, y_t | s'_{t-1}, x_t) = p_{S'_t | S'_{t-1}, X_t}(s'_t | s'_{t-1}, x_t) \cdot p_{Y_t | S'_{t-1}, X_t}(y_t | s'_{t-1}, x_t),$$

where

$$p_{S'_t | S'_{t-1}, X_t}(s'_t | s'_{t-1}, x_t) \triangleq \mathbb{1}(s'_t = \mathbf{x}_{t-m+1}^t) \cdot \mathbb{1}(s'_{t-1} = \mathbf{x}_{t-m}^{t-1}),$$

$$p_{Y_t | S'_{t-1}, X_t}(y_t | s'_{t-1}, x_t) \triangleq \frac{1}{\sqrt{2\pi\sigma^2}} \cdot \exp\left(-\frac{(y_t - u_t)^2}{2\sigma^2}\right),$$

with $u_t \triangleq \sum_{\ell=0}^m g_\ell x_{t-\ell}$ and $\mathbf{x}_{t-m}^{t-1} = s'_{t-1}$.

All possible state sequences of an ISI channel (and more generally, of an FSMC) can be represented by a trellis diagram. Because of the assumed time-invariance, it is sufficient to show a single trellis section. For example, Fig. 2(b) shows a trellis section of an ISI channel characterized by the couple $(g(D) \triangleq 1 - D, \sigma^2)$, known as a dicode channel, with an input alphabet $\mathcal{X} \triangleq \{+1, -1\}$. In this diagram, branches start at state s'_{t-1} , end at state s'_t , and have noiseless channel output symbol u_t shown next to them.

Definition 5 (Intersymbol Interference Wiretap Channel (ISI-WTC)). In an ISI-WTC, Alice transmits data symbols over Bob's channel and over Eve's channel, which are both assumed to be ISI channels with finite input alphabet $\mathcal{X} \subsetneq \mathbb{R}$. Specifically, Bob's channel is an ISI channel described by the couple $(g^B(D), \sigma_B^2)$, with transfer polynomial $g^B(D) = \sum_{t=0}^{m_B} g_t^B D^t$, noiseless output process $\{U_t\}_{t \in \mathbb{Z}}$, noise process $\{N_t^B\}_{t \in \mathbb{Z}}$, and noisy output process $\{Y_t\}_{t \in \mathbb{Z}}$. Similarly, Eve's channel is an ISI channel described by the couple $(g^E(D), \sigma_E^2)$, with transfer polynomial $g^E(D) = \sum_{t=0}^{m_E} g_t^E D^t$, noiseless output process $\{V_t\}_{t \in \mathbb{Z}}$, noise process $\{N_t^E\}_{t \in \mathbb{Z}}$, and noisy output process $\{Z_t\}_{t \in \mathbb{Z}}$. We assume that the noise process of Bob's channel and the noise process of Eve's channel are independent. Clearly, the ISI-WTC is parameterized by the quadruple $(g^B(D), g^E(D), \sigma_B^2, \sigma_E^2)$. \square

Definition 6 (Finite-State Joint Source Wiretap Channel (FS-JSWTC)). We define an FS-JSWTC model based on the concatenation of the following components; an FSMS as in Remark 2 described by the triple $(\mathcal{X}, \bar{\nu}, p_{X_t|X_{t-\bar{\nu}}^{t-1}}(x_t|\mathbf{x}_{t-\bar{\nu}}^{t-1}))$, where \mathcal{X} is a finite subset of \mathbb{R} , and an ISI-WTC as in Definition 5 described by the quadruple $(g^B(D), g^E(D), \sigma_B^2, \sigma_E^2)$. \square

Note that an FS-JSWTC can be modeled by a single (time-invariant) finite-state machine. Namely, letting

$$\nu \triangleq \max(\bar{\nu}, m_B, m_E), \quad (1)$$

where m_B and m_E are the degrees of $g^B(D)$ and $g^E(D)$, respectively, the state space is given by $\mathcal{S} \triangleq \mathcal{X}^\nu$ and the state at time $t \in \mathbb{Z}$ is given by $S_t \triangleq \mathbf{X}_{t-\nu+1}^t \in \mathcal{S}$.

Assumption 7. In the following, we will consider the FSMSs where $\bar{\nu} \geq m_B$ and $\bar{\nu} \geq m_E$, which implies that $\nu = \max(\bar{\nu}, m_B, m_E) = \bar{\nu}$.³ \square

³With a suitable notation, the case $\bar{\nu} < \max(m_B, m_E)$ can be handled.

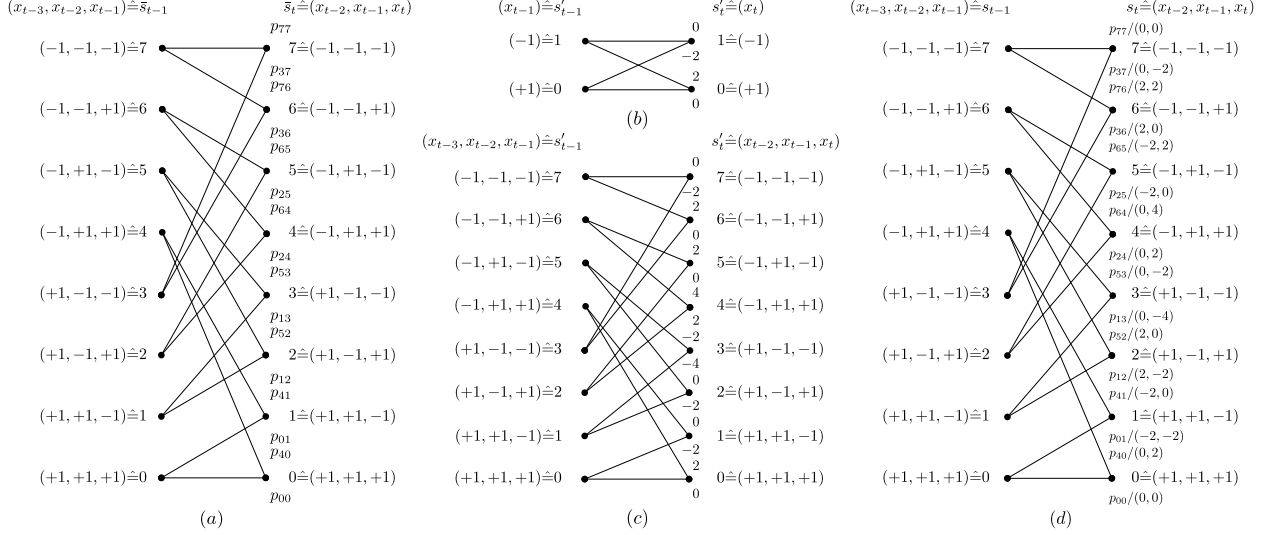


Fig. 2: (a) Trellis section of an FSMS with $\mathcal{X} = \{+1, -1\}$ and memory order $\bar{\nu} = 3$. State transition probabilities are shown next to branches. (b) Trellis section of a decode channel (i.e., an ISI channel with $g(D) = 1 - D$) when used with input alphabet $\mathcal{X} = \{+1, -1\}$. The noiseless channel output symbol is shown next to branches. (c) Trellis section of an EPR4 channel (i.e., an ISI channel with $g(D) = 1 + D - D^2 - D^3$) when used with input alphabet $\mathcal{X} = \{+1, -1\}$. The noiseless channel output symbol is shown next to branches. (d) Trellis section of an FS-JSWTC comprised of a third-order FSMS, a decode channel to Bob, and an EPR4 channel to Eve. State transition probabilities and noiseless channel output symbols (one noiseless channel output symbol for Bob's channel, one noiseless channel output symbol for Eve's channel) are shown next to branches.

Thanks to Assumption 7, the state transition probabilities of the finite-state machine modeling the FS-JSWTC will be the same as the state transition probabilities of the FSMS.

Definition 8. Let \mathcal{B} denote the set of all valid consecutive state pairs $(s_{t-1}, s_t) \in \mathcal{S} \times \mathcal{S}$ for any $t \in \mathbb{Z}$. Moreover, let

$$\vec{\mathcal{S}}_i \triangleq \{j \mid (i, j) \in \mathcal{B}\}, \quad \overleftarrow{\mathcal{S}}_j \triangleq \{i \mid (i, j) \in \mathcal{B}\}$$

be the set of states S_t reachable from state $S_{t-1} = i$ and the set of states S_{t-1} that can reach $S_t = j$, respectively. \square

Definition 9. For $(i, j) \in \mathcal{B}$, let $p_{ij} \triangleq p_{S_t|S_{t-1}}(j|i)$ be the time-invariant probability of going from state $S_{t-1} = i$ to state $S_t = j$ for any $t \in \mathbb{Z}$. We assume that $\{p_{ij}\}_{(i,j) \in \mathcal{B}}$ is corresponding to an ergodic FSMS, and so there is a unique stationary state probability distribution $\{\mu_i\}_{i \in \mathcal{S}}$, i.e., $p_{S_t}(i) = \mu_i$ for all $t \in \mathbb{Z}$. Accordingly, let $\{Q_{ij}\}_{(i,j) \in \mathcal{B}}$ be defined by $Q_{ij} \triangleq \mu_i \cdot p_{ij}$, for all $(i, j) \in \mathcal{B}$. \square

In the above definition, we started with $\{p_{ij}\}_{(i,j) \in \mathcal{B}}$ and derived $\{\mu_i\}_{i \in \mathcal{S}}$ and $\{Q_{ij}\}_{(i,j) \in \mathcal{B}}$

from it. However, for analytical purposes, it turns out to be beneficial to start with $\{Q_{ij}\}_{(i,j) \in \mathcal{B}}$ and derive $\{p_{ij}\}_{(i,j) \in \mathcal{B}}$ and $\{\mu_i\}_{i \in \mathcal{S}}$ from $\{Q_{ij}\}_{(i,j) \in \mathcal{B}}$. Note that the set of all $\{Q_{ij}\}_{(i,j) \in \mathcal{B}}$ is given by the polytope $\mathcal{Q}(\mathcal{B})$, where

$$\mathcal{Q}(\mathcal{B}) \triangleq \left\{ \{Q_{ij}\}_{(i,j) \in \mathcal{B}} \mid Q_{ij} \geq 0, \forall (i,j) \in \mathcal{B}; \sum_{(i,j) \in \mathcal{B}} Q_{ij} = 1; \sum_{j \in \vec{\mathcal{S}}_i} Q_{ij} = \sum_{k \in \overleftarrow{\mathcal{S}}_i} Q_{ki}, \forall i \in \mathcal{S} \right\}.$$

In the following, we will use the short-hand notation \mathbf{Q} for $\{Q_{ij}\}_{(i,j) \in \mathcal{B}}$.

Example 10. Consider an FS-JSWTC, where the FSMS as in Remark 2 is described by the triple $(\mathcal{X}, \bar{\nu}, p_{X_t|X_{t-\bar{\nu}}^{t-1}}(x_t|\mathbf{x}_{t-\bar{\nu}}^{t-1}))$ with $\mathcal{X} = \{+1, -1\}$ and $\bar{\nu} = 3$ (see Fig. 2(a)); where Bob's channel is a decode channel, i.e., $g^B(D) = 1 - D$ (see Fig. 2(b)); and where Eve's channel is an EPR4 channel, i.e., $g^E(D) = 1 + D - D^2 - D^3$ (see Fig. 2(c)). This setup satisfies Assumption 7 and so $\nu = \bar{\nu} = 3$. All possible state sequences of an FS-JSWTC can be represented by a trellis diagram. Because of the assumed time-invariance, it is sufficient to show a single trellis section, as is shown in Fig. 2(d) for the present example. \square

Remark 11 (Parameterized family of \mathbf{Q}). Frequently, we will consider the setup where $\mathbf{Q}(\theta)$ is a function of some parameter θ . More precisely, for every $(i,j) \in \mathcal{B}$, we let $Q_{ij}(\theta)$ be a smooth function of some parameter θ , where θ varies over a suitable range. We require for every θ it holds that $\mathbf{Q}(\theta) = \{Q_{ij}(\theta)\}_{(i,j) \in \mathcal{B}} \in \mathcal{Q}(\mathcal{B})$. For every $(i,j) \in \mathcal{B}$, we denote the derivative of $Q_{ij}(\theta)$ w.r.t. θ and evaluated at $\tilde{\theta}$ by $Q_{ij}^\theta(\tilde{\theta})$. In accordance, the steady-state and the transition probabilities parameterized by θ are denoted by $\mu_i(\theta)$ and $p_{ij}(\theta)$, respectively. Similarly, their derivatives w.r.t. θ and evaluated at $\tilde{\theta}$ are denoted by $\mu_i^\theta(\tilde{\theta})$ and $p_{ij}^\theta(\tilde{\theta})$, respectively. Obviously, we have $\sum_{(i,j) \in \mathcal{B}} Q_{ij}^\theta(\tilde{\theta}) = 0$, $\sum_{i \in \mathcal{S}} \mu_i^\theta(\tilde{\theta}) = 0$. \square

Remark 12. Some technical remarks concerning the considered setup:

- It is well known that ISI channels are indecomposable FSMCs [14], which means that the influence of the initial state vanishes over time. This implies that the information rates being well defined even if the initial state is not known.
- Algorithm 2 in Section IV will make use of Perron–Frobenius theory for irreducible non-negative matrices. One can verify that the relevant matrix is indeed irreducible, except for uninteresting boundary cases. \square

III. SECURE RATE: ACHIEVABILITY AND ESTIMATION

In what follows, Section III-A gives a concise presentation of the employed secrecy criterion in this study. Relying on this criterion, Section III-B establishes a lower bound on the achievable secure information rates over ISI-WTCs. Accordingly, a numerical estimation of the obtained secure rates is presented in Section III-C.

A. Secrecy Criterion

Let M_n be a random variable corresponding to a uniformly chosen secret message from an alphabet \mathcal{M}_n . Also, let \mathbf{Z}_1^n denote an encoded (noisy) sequence that captures Eve's knowledge about M_n (see Fig. 1). The statistical independence between M_n and \mathbf{Z}_1^n is often measured by the mutual information to ensure the information-theoretic perfect secrecy. For instance, the so-called strong secrecy criterion [30] requires $\lim_{n \rightarrow \infty} I(M_n; \mathbf{Z}_1^n) = 0$, and the so-called weak secrecy criterion [31] requires $\lim_{n \rightarrow \infty} \frac{1}{n} I(M_n; \mathbf{Z}_1^n) = 0$. It should be noted that the weak secrecy criterion could be satisfied through vulnerable coding schemes with evident security flaws [32, Ch. 3.3]. Hence, it is not suitable for assuring the secrecy. On the other hand, satisfying the extremely stringent independence condition in the strong secrecy criterion is impossible for most of the practical coding schemes [33]. This trade-off between tractability and strength led us to employ the secrecy criterion

$$\lim_{n \rightarrow \infty} d_{\mathcal{M}_n \times \mathcal{Z}^n}(p_{M_n, \mathbf{Z}_1^n}, p_{M_n} p_{\mathbf{Z}_1^n}) = 0, \quad (2)$$

which is stronger than the weak secrecy criterion and is more relaxed compared with the strong secrecy criterion [33, Lemma 1]. Rewording of the mentioned secrecy metric leads to

$$\begin{aligned} d_{\mathcal{M}_n \times \mathcal{Z}^n}(p_{M_n, \mathbf{Z}_1^n}, p_{M_n} p_{\mathbf{Z}_1^n}) &= \int_{\mathbf{z}_1^n \in \mathcal{Z}^n} \sum_{m_n \in \mathcal{M}_n} p_{M_n}(m_n) \cdot \left| p_{\mathbf{Z}_1^n | M_n}(\mathbf{z}_1^n | m_n) - p_{\mathbf{Z}_1^n}(\mathbf{z}_1^n) \right| d\mathbf{z}_1^n \\ &= \int_{\mathbf{z}_1^n \in \mathcal{Z}^n} \sum_{m_n \in \mathcal{M}_n} p_{M_n}(m_n) \cdot \left| p_{\mathbf{Z}_1^n | M_n}(\mathbf{z}_1^n | m_n) - \sum_{m'_n \in \mathcal{M}_n} p_{\mathbf{Z}_1^n, M_n}(\mathbf{z}_1^n, m'_n) \right| d\mathbf{z}_1^n \\ &= \sum_{(m_n, m'_n) \in \mathcal{M}_n^2} p_{M_n}(m_n) \cdot p_{M_n}(m'_n) \cdot \int_{\mathbf{z}_1^n \in \mathcal{Z}^n} \left| p_{\mathbf{Z}_1^n | M_n}(\mathbf{z}_1^n | m_n) - p_{\mathbf{Z}_1^n | M_n}(\mathbf{z}_1^n | m'_n) \right| d\mathbf{z}_1^n \\ &= \sum_{(m_n, m'_n) \in \mathcal{M}_n^2} p_{M_n}(m_n) \cdot p_{M_n}(m'_n) \cdot d_{\mathcal{Z}^n}(p_{\mathbf{Z}_1^n | M_n=m_n}, p_{\mathbf{Z}_1^n | M_n=m'_n}). \end{aligned} \quad (3)$$

It follows from (3) that satisfying (2) makes $m_n, m'_n \in \mathcal{M}_n$ statistically indistinguishable at Eve's decoder. The formulation in (3) implies a relaxed notion of distinguishing security

criterion in cryptography [34], requiring

$$\max_{(m_n, m'_n) \in \mathcal{M}_n^2} \left(d_{\mathcal{Z}^n}(p_{\mathbf{Z}_1^n | M_n = m_n}, p_{\mathbf{Z}_1^n | M_n = m'_n}) \right) = 0.$$

The distinguishing security criterion is equivalent to the well-known formulation of the semantic security⁴ [34]. Hence, satisfying the secrecy criterion (2) gives rise to a loosened notion of the semantic security. This looseness arises from the extra assumption that $p_{M_n}(m_n)$ is known, for all $m_n \in M_n$, contrary to the cryptographically relevant secrecy criteria.

B. Secure Rate: Achievability

Following from [35], the spectral sup/inf-mutual information rates are defined to be

$$\begin{aligned} \text{p-lim sup}_{n \rightarrow \infty} \frac{1}{n} i(\mathbf{X}_1^n; \mathbf{Y}_1^n) &\triangleq \inf \left\{ \alpha : \lim_{n \rightarrow \infty} \Pr \left(\frac{1}{n} i(\mathbf{X}_1^n; \mathbf{Y}_1^n) > \alpha \right) = 0 \right\}, \\ \text{p-lim inf}_{n \rightarrow \infty} \frac{1}{n} i(\mathbf{X}_1^n; \mathbf{Y}_1^n) &\triangleq \sup \left\{ \beta : \lim_{n \rightarrow \infty} \Pr \left(\frac{1}{n} i(\mathbf{X}_1^n; \mathbf{Y}_1^n) < \beta \right) = 0 \right\}. \end{aligned}$$

Lemma 13. [36, Lemma 2] For an arbitrary wiretap channel $(\mathcal{X}, \{p_{\mathbf{Y}_1^n, \mathbf{Z}_1^n | \mathbf{X}_1^n}(\mathbf{y}_1^n, \mathbf{z}_1^n | \mathbf{x}_1^n)\}_{n=1}^\infty, \mathcal{Y}, \mathcal{Z})$ consisting of an arbitrary input alphabet \mathcal{X} , two arbitrary output alphabets \mathcal{Y} and \mathcal{Z} corresponding to Bob's and Eve's observations, respectively, and a sequence of transition probabilities $\{p_{\mathbf{Y}_1^n, \mathbf{Z}_1^n | \mathbf{X}_1^n}(\mathbf{y}_1^n, \mathbf{z}_1^n | \mathbf{x}_1^n)\}_{n=1}^\infty$, all secure rates R_s satisfying

$$R_s < \max_{\{\mathbf{X}_1^n\}_{n=1}^\infty} \left(\text{p-lim inf}_{n \rightarrow \infty} \frac{1}{n} i(\mathbf{X}_1^n; \mathbf{Y}_1^n) - \text{p-lim sup}_{n \rightarrow \infty} \frac{1}{n} i(\mathbf{X}_1^n; \mathbf{Z}_1^n) \right)$$

are achievable under the secrecy criterion (2) and the reliability criterion

$$\limsup_{n \rightarrow \infty} \epsilon_n = 0, \tag{4}$$

where ϵ_n is the probability of error at Bob's decoder for a block of length n .

Lemma 13 can be leveraged to deduce the following achievability result for ISI-WTCs.

Proposition 14. Consider some ISI-WTC with an input alphabet \mathcal{X} described by the quadruple $(g^B(D), g^E(D), \sigma_B^2, \sigma_E^2)$. For all positive integers ℓ and $\nu \geq \max(m_B, m_E)$, and any input

⁴Operationally, under the semantic secrecy criterion, it is impossible for Eve to estimate any function of M_n better than to guess it without considering \mathbf{Z}_1^n .

distribution $p_{\mathbf{X}_{-\nu+1}^\ell}$, all secure rates R_s satisfying

$$R_s < \frac{1}{\ell + 2\nu} \left(I(\mathbf{X}_1^\ell; \mathbf{Y}_1^\ell | \mathbf{X}_{-\nu+1}^0) - I(\mathbf{X}_1^\ell; \mathbf{Z}_1^\ell | \mathbf{X}_{-\nu+1}^0) - 3\nu \cdot \log |\mathcal{X}| \right)$$

are achievable under the the secrecy criterion (2) and the reliability criterion (4).

Proof. See Appendix A. □

Definition 15. Consider an FS-JSWTC with an FSMS described by \mathbf{Q} . We define

$$R_s(\mathbf{Q}) \triangleq \lim_{n \rightarrow \infty} \frac{1}{n} \left(I(\mathbf{S}_1^n; \mathbf{Y}_1^n | S_0) - I(\mathbf{S}_1^n; \mathbf{Z}_1^n | S_0) \right). \quad (5)$$

□

Corollary 16. Consider an FS-JSWTC with an FSMS described by \mathbf{Q} . All secure rates R_s satisfying

$$R_s < R_s(\mathbf{Q})$$

are achievable under the secrecy (2) and the reliability (4) criteria.

Proof. Let ν be the memory of the associated FS-JSWTC (see (1)). It is easy to verify that

$$I(\mathbf{X}_1^n; \mathbf{Y}_1^n | \mathbf{X}_{-\nu+1}^0) = I(\mathbf{S}_1^n; \mathbf{Y}_1^n | S_0),$$

$$I(\mathbf{X}_1^n; \mathbf{Z}_1^n | \mathbf{X}_{-\nu+1}^0) = I(\mathbf{S}_1^n; \mathbf{Z}_1^n | S_0).$$

Invoking Proposition 14 and letting $n \rightarrow \infty$ proves the promised result. □

We are now in a position to introduce the notion of constrained secrecy capacity, which is a key quantity to be studied in the subsequent parts of this paper.

Definition 17. Consider an FS-JSWTC as in Definition 6, where the FSMS described by \mathbf{Q} can vary in $\mathcal{Q}(\mathcal{B})$. The constrained secrecy capacity (or, more precisely, the $\mathcal{Q}(\mathcal{B})$ -constrained secrecy capacity) is defined as

$$C_{\mathcal{Q}(\mathcal{B})} \triangleq \max_{\mathbf{Q} \in \mathcal{Q}(\mathcal{B})} R_s(\mathbf{Q}).$$

□

C. Secure Rate: Estimation

Throughout this section, we consider an FS-JSWTC as in Definition 6, where the FSMS is described by $\mathbf{Q} \in \mathcal{Q}(\mathcal{B})$. The secure rate in $R_s(\mathbf{Q})$ can be efficiently estimated using variants of the algorithms in [37]. (We omit the details.) The main purpose of this section is to present an alternative approach for estimating $R_s(\mathbf{Q})$. Although the resulting algorithms by themselves are slightly less efficient than the estimation algorithms based on [37], they are based on quantities that need to be calculated as part of the optimization algorithm presented in the next section. Therefore, when running these optimization algorithms, these quantities are readily available and can be used to estimate $R_s(\mathbf{Q})$.

Definition 18. Consider an FS-JSWTC with an FSMS described by \mathbf{Q} . We define

$$T_{ij}^B(\mathbf{Q}) \triangleq \lim_{n \rightarrow \infty} \int_{\mathbf{y}_1^n \in \mathcal{Y}^n} p_{\mathbf{Y}_1^n}(\mathbf{y}_1^n) \cdot \check{T}_{ij}^B(\mathbf{Q}, \mathbf{y}_1^n) d\mathbf{y}_1^n, \quad (6)$$

$$T_{ij}^E(\mathbf{Q}) \triangleq \lim_{n \rightarrow \infty} \int_{\mathbf{z}_1^n \in \mathcal{Z}^n} p_{\mathbf{Z}_1^n}(\mathbf{z}_1^n) \cdot \check{T}_{ij}^E(\mathbf{Q}, \mathbf{z}_1^n) d\mathbf{z}_1^n, \quad (7)$$

where

$$\check{T}_{ij}^B(\mathbf{Q}, \mathbf{y}_1^n) \triangleq \frac{1}{n} \sum_{t=1}^n \log \left(\frac{p_{S_{t-1}, S_t | \mathbf{Y}_1^n}(i, j | \mathbf{y}_1^n)^{p_{S_{t-1}, S_t | \mathbf{Y}_1^n}(i, j | \mathbf{y}_1^n) / \mu_i p_{ij}}}{p_{S_{t-1} | \mathbf{Y}_1^n}(i | \mathbf{y}_1^n)^{p_{S_{t-1} | \mathbf{Y}_1^n}(i | \mathbf{y}_1^n) / \mu_i}} \right), \quad (8)$$

$$\check{T}_{ij}^E(\mathbf{Q}, \mathbf{z}_1^n) \triangleq \frac{1}{n} \sum_{t=1}^n \log \left(\frac{p_{S_{t-1}, S_t | \mathbf{Z}_1^n}(i, j | \mathbf{z}_1^n)^{p_{S_{t-1}, S_t | \mathbf{Z}_1^n}(i, j | \mathbf{z}_1^n) / \mu_i p_{ij}}}{p_{S_{t-1} | \mathbf{Z}_1^n}(i | \mathbf{z}_1^n)^{p_{S_{t-1} | \mathbf{Z}_1^n}(i | \mathbf{z}_1^n) / \mu_i}} \right), \quad (9)$$

for every $(i, j) \in \mathcal{B}$.⁵ □

Proposition 19 (Secure information rate). The secure rate of the FS-JSWTC with an FSMS described by \mathbf{Q} can be expressed as

$$R_s(\mathbf{Q}) = \sum_{(i,j) \in \mathcal{B}} Q_{ij} \cdot (T_{ij}^B(\mathbf{Q}) - T_{ij}^E(\mathbf{Q})).$$

Proof. See Appendix B. □

⁵The expressions T_{ij}^B and T_{ij}^E are similar to the expression for $\check{T}_{ij}^{(N)}$ in [17, Lemma 70], part “second possibility.”

Algorithm 1 Secure Rate Estimation

Input: FSMS distribution \mathbf{Q}

- 1: Generate a sequence $\check{\mathbf{x}}_1^n$ based on the FSMS \mathbf{Q} ;
 - 2: Simulate Bob's (Eve's) channel with $\check{\mathbf{x}}_1^n$ at the input to obtain $\check{\mathbf{y}}_1^n$ ($\check{\mathbf{z}}_1^n$) at the output;
 - 3: Calculate $\check{T}_{ij}^B(\mathbf{Q}, \check{\mathbf{y}}_1^n)$ and $\check{T}_{ij}^E(\mathbf{Q}, \check{\mathbf{z}}_1^n)$ using (8) and (9) with the help of variants of the sum-product / BCJR algorithm [17];
 - 4: $\check{R}_s(\mathbf{Q}) \leftarrow \sum_{(i,j) \in \mathcal{B}} Q_{ij} \cdot (\check{T}_{ij}^B(\mathbf{Q}, \check{\mathbf{y}}_1^n) - \check{T}_{ij}^E(\mathbf{Q}, \check{\mathbf{z}}_1^n))$;
 - 5: **return** $R_s(\mathbf{Q})$
-

Remark 20. The reformulation of the secure rate in Proposition 19 can be used to efficiently estimate $R_s(\mathbf{Q})$ as shown in Algorithm 1.⁶

IV. SECURE RATE: OPTIMIZATION

Throughout this section, we consider an FS-JSWTC as in Definition 6, where the FSMS described by \mathbf{Q} varies in $\mathcal{Q}(\mathcal{B})$. Note that, $R_s(\mathbf{Q})$ is not a closed-form function in terms of \mathbf{Q} and its evaluation is only possible through the Monte-Carlo methods as in Algorithm 1. Moreover, $R_s(\mathbf{Q})$ is a highly fluctuating non-concave function according to our numerical simulations. Consequently, the optimization problem appearing in the specification of the constrained secrecy capacity in Definition 17 turns out to be intractable in general. Given this, we focus on efficient algorithms for finding a local maximum of $R_s(\mathbf{Q})$ in this section. We formulate an iterative optimization method inspired by the expectation-maximization (EM) algorithm. Namely, the proposed algorithm at every iteration approximates the function $R_s(\mathbf{Q})$ by a suitable surrogate function that is well-defined over $\mathcal{Q}(\mathcal{B})$ and can be efficiently maximized. Related techniques were also used in [17], [38].

A. Outline of the Optimization Algorithm

The proposed algorithm is an iterative algorithm that works as follows

- Assume that at the current iteration the algorithm has found the FSMS described by $\tilde{\mathbf{Q}} \triangleq \{\tilde{Q}_{ij}\}_{(i,j) \in \mathcal{B}}$.
- Around $\mathbf{Q} = \tilde{\mathbf{Q}}$, we approximate the function $R_s(\mathbf{Q})$ over $\mathcal{Q}(\mathcal{B})$ by the surrogate function $\psi_{\tilde{\mathbf{Q}}}(\mathbf{Q})$ over $\mathcal{Q}(\mathcal{B})$ satisfying the following properties:

⁶The accuracy of the approximation can be controlled by choosing n suitably large.

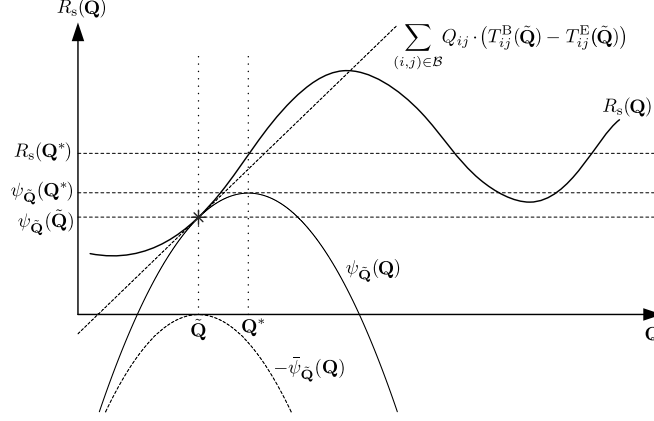


Fig. 3: Sketch of the functions appearing in the optimization algorithm discussed in Section IV.

- The value of $\psi_{\tilde{\mathbf{Q}}}(\mathbf{Q})$ matches the value of $R_s(\mathbf{Q})$ at $\mathbf{Q} = \tilde{\mathbf{Q}}$.
- The gradient of $\psi_{\tilde{\mathbf{Q}}}(\mathbf{Q})$ w.r.t. \mathbf{Q} matches the gradient of $R_s(\mathbf{Q})$ w.r.t. \mathbf{Q} at $\mathbf{Q} = \tilde{\mathbf{Q}}$.
- The function $\psi_{\tilde{\mathbf{Q}}}(\mathbf{Q})$ is concave in \mathbf{Q} and can be efficiently maximized.
- Replace $\tilde{\mathbf{Q}}$ by the \mathbf{Q} maximizing $\psi_{\tilde{\mathbf{Q}}}(\mathbf{Q})$.

A sketch of these functions is shown in Fig. 3.

In the following, in the same way that we derived $\{p_{ij}\}_{(i,j) \in \mathcal{B}}$ and $\{\mu_i\}_{i \in \mathcal{S}}$ from $\mathbf{Q} = \{Q_{ij}\}_{(i,j) \in \mathcal{B}}$, we will derive $\{\tilde{p}_{ij}\}_{(i,j) \in \mathcal{B}}$ and $\{\tilde{\mu}_i\}_{i \in \mathcal{S}}$ from $\tilde{\mathbf{Q}} = \{\tilde{Q}_{ij}\}_{(i,j) \in \mathcal{B}}$.

B. The Surrogate Function and its Properties

Definition 21 (Surrogate function). The surrogate function based on $\tilde{\mathbf{Q}}$ is defined to be

$$\psi_{\tilde{\mathbf{Q}}}(\mathbf{Q}) \triangleq \sum_{(i,j) \in \mathcal{B}} Q_{ij} \cdot (T_{ij}^{\mathcal{B}}(\tilde{\mathbf{Q}}) - T_{ij}^{\mathcal{E}}(\tilde{\mathbf{Q}})) - \bar{\psi}_{\tilde{\mathbf{Q}}}(\mathbf{Q}), \quad (10)$$

where

$$\bar{\psi}_{\tilde{\mathbf{Q}}}(\mathbf{Q}) \triangleq \kappa' \cdot \left(\sum_{(i,j) \in \mathcal{B}} \tilde{Q}_{ij} \cdot (1 + \kappa \cdot (\delta Q)_{ij}) \cdot \log(1 + \kappa \cdot (\delta Q)_{ij}) - \sum_{i \in \mathcal{S}} \tilde{\mu}_i \cdot (1 + \kappa \cdot (\delta \mu)_i) \cdot \log(1 + \kappa \cdot (\delta \mu)_i) \right).$$

Here, for every $(i, j) \in \mathcal{B}$, the quantities $(\delta Q)_{ij}$ and $(\delta \mu)_i$ are defined to be, respectively,

$$(\delta Q)_{ij} \triangleq \frac{Q_{ij} - \tilde{Q}_{ij}}{\tilde{Q}_{ij}}, \quad (\delta \mu)_i \triangleq \frac{\mu_i - \tilde{\mu}_i}{\tilde{\mu}_i}.$$

Furthermore, the real parameters $0 < \kappa \leq 1$ and $\kappa' > 0$ are used to control the shape of $\bar{\psi}_{\tilde{\mathbf{Q}}}(\mathbf{Q})$, and with that the shape of $\psi_{\tilde{\mathbf{Q}}}(\mathbf{Q})$. (These parameters can be used to control the aggressiveness of the search step size.) \square

Assumption 22. In order to show that the surrogate function $\psi_{\tilde{\mathbf{Q}}}(\mathbf{Q})$ in Definition 21 has the promised properties, we consider a parameterization $\mathbf{Q}(\theta)$ of \mathbf{Q} as discussed in Remark 11. We assume that the parameterization is smooth and there is a $\tilde{\theta}$ such that $\tilde{\mathbf{Q}} = \mathbf{Q}(\tilde{\theta})$. \square

In the following, we will use the short-hand notations $R_s(\theta)$ and $\psi_{\tilde{\mathbf{Q}}}(\theta)$ for $R_s(\mathbf{Q}(\theta))$ and $\psi_{\tilde{\mathbf{Q}}}(\mathbf{Q}(\theta))$, respectively.

Lemma 23 (Property 1 of the surrogate function ψ). The value of $\psi_{\tilde{\mathbf{Q}}}(\mathbf{Q})$ matches the value of $R_s(\mathbf{Q})$ at $\mathbf{Q} = \tilde{\mathbf{Q}}$, i.e.,

$$\psi_{\tilde{\mathbf{Q}}}(\tilde{\mathbf{Q}}) = R_s(\tilde{\mathbf{Q}}),$$

and, in terms of the parameterization defined above,

$$\psi_{\tilde{\mathbf{Q}}}(\tilde{\theta}) = R_s(\tilde{\theta}).$$

Proof. We start by noting that $\mathbf{Q} = \tilde{\mathbf{Q}}$ implies that $(\delta Q)_{ij} = 0$ and $(\delta \mu)_i = 0$ for all $(i, j) \in \mathcal{B}$, which in turn implies that $\bar{\psi}_{\tilde{\mathbf{Q}}}(\tilde{\mathbf{Q}}) = 0$. The result $\psi_{\tilde{\mathbf{Q}}}(\tilde{\mathbf{Q}}) = R_s(\tilde{\mathbf{Q}})$ follows then from the definition of $\psi_{\tilde{\mathbf{Q}}}(\mathbf{Q})$ in Definition 21, along with Proposition 19. \square

Lemma 24 (Property 2 of the surrogate function ψ). The gradient of $\psi_{\tilde{\mathbf{Q}}}(\mathbf{Q})$ w.r.t. \mathbf{Q} matches the gradient of $R_s(\mathbf{Q})$ w.r.t. \mathbf{Q} at $\mathbf{Q} = \tilde{\mathbf{Q}}$, i.e.,

$$\left. \frac{d}{d\theta} \psi_{\tilde{\mathbf{Q}}}(\theta) \right|_{\theta=\tilde{\theta}} = \left. \frac{d}{d\theta} R_s(\theta) \right|_{\theta=\tilde{\theta}}$$

for any parameterization as defined above.

Proof. We start by showing that

$$\left. \frac{d}{d\theta} \bar{\psi}_{\tilde{\mathbf{Q}}}(\theta) \right|_{\theta=\tilde{\theta}} = 0. \tag{11}$$

Indeed,

$$\begin{aligned} \left. \frac{d}{d\theta} \bar{\psi}_{\tilde{\mathbf{Q}}}(\theta) \right|_{\theta=\tilde{\theta}} &= \kappa \kappa' \cdot \left(\sum_{(i,j) \in \mathcal{B}} Q_{ij}^{\theta}(\tilde{\theta}) \cdot \log(1 + \kappa \cdot (\delta Q(\tilde{\theta}))_{ij}) - \sum_{i \in \mathcal{S}} \mu_i^{\theta}(\tilde{\theta}) \cdot \log(1 + \kappa \cdot (\delta \mu(\tilde{\theta}))_i) \right) \Big|_{\theta=\tilde{\theta}} \\ &= 0. \end{aligned}$$

We then have

$$\begin{aligned} \left. \frac{d}{d\theta} \psi_{\tilde{\mathbf{Q}}}(\theta) \right|_{\theta=\tilde{\theta}} &= \left. \frac{d}{d\theta} (\psi_{\tilde{\mathbf{Q}}}(\theta) + \bar{\psi}_{\tilde{\mathbf{Q}}}(\theta)) \right|_{\theta=\tilde{\theta}} = \left. \frac{d}{d\theta} \left(\sum_{(i,j) \in \mathcal{B}} Q_{ij}(\theta) \cdot (T_{ij}^{\mathbf{B}}(\tilde{\theta}) - T_{ij}^{\mathbf{E}}(\tilde{\theta})) \right) \right|_{\theta=\tilde{\theta}} \\ &= \left. \frac{d}{d\theta} \left(\sum_{(i,j) \in \mathcal{B}} Q_{ij}(\theta) \cdot (T_{ij}^{\mathbf{B}}(\theta) - T_{ij}^{\mathbf{E}}(\theta)) \right) \right|_{\theta=\tilde{\theta}} = \left. \frac{d}{d\theta} R_s(\theta) \right|_{\theta=\tilde{\theta}}, \end{aligned}$$

where the first equality follows from (11), where the second equality from Definition 21, where the third equality follows from [17, Lemma 64], and where the fourth equality follows from Proposition 19. \square

Remark 25. Despite the close similarity between the third and fourth expression in the final display equation of the above proof, this is a non-trivial result because of the non-triviality of [17, Lemma 64].

Lemma 26 (Convexity of the function $\bar{\psi}_{\tilde{\mathbf{Q}}}$). The function $\bar{\psi}_{\tilde{\mathbf{Q}}}(\mathbf{Q})$ is convex over $\mathbf{Q} \in \mathcal{Q}(\mathcal{B})$.

Proof. See Appendix C. \square

Lemma 27 (Concavity of the surrogate function $\psi_{\tilde{\mathbf{Q}}}$). The surrogate function $\psi_{\tilde{\mathbf{Q}}}(\mathbf{Q})$ is concave over $\mathbf{Q} \in \mathcal{Q}(\mathcal{B})$.

Proof. This follows immediately from Lemma 26 and from $\sum_{(i,j) \in \mathcal{B}} Q_{ij} \cdot (T_{ij}^{\mathbf{B}}(\tilde{\mathbf{Q}}) - T_{ij}^{\mathbf{E}}(\tilde{\mathbf{Q}}))$ being a linear function of \mathbf{Q} . \square

C. Maximizing the Surrogate Function

Let $\tilde{\mathbf{Q}}$ denote the FSMS distribution attained at the current iteration of the proposed algorithm. For the next iteration, $\tilde{\mathbf{Q}}$ is replaced by $\mathbf{Q}^* = \{Q_{ij}^*\}_{(i,j) \in \mathcal{B}}$, where

$$\mathbf{Q}^* \triangleq \arg \max_{\mathbf{Q} \in \mathcal{Q}(\mathcal{B})} \psi_{\tilde{\mathbf{Q}}}(\mathbf{Q}). \quad (12)$$

In the following, in the same way that we derived $\{p_{ij}\}_{(i,j) \in \mathcal{B}}$ and $\{\mu_i\}_{i \in \mathcal{S}}$ from $\mathbf{Q} = \{Q_{ij}\}_{(i,j) \in \mathcal{B}}$, we will derive $\{p_{ij}^*\}_{(i,j) \in \mathcal{B}}$ and $\{\mu_i^*\}_{i \in \mathcal{S}}$ from $\mathbf{Q}^* = \{Q_{ij}^*\}_{(i,j) \in \mathcal{B}}$.

Proposition 28 (The optimum distribution \mathbf{Q}^).* The optimum FSMS distribution \mathbf{Q}^* in (12) is calculated as follows. Let $\mathbf{A} \triangleq (A_{ij})_{i,j \in \mathcal{S}}$ be the matrix with entries

$$A_{ij} \triangleq \begin{cases} \tilde{p}_{ij} \cdot \exp\left(\frac{\tilde{T}_{ij}^{\mathbf{B}} - \tilde{T}_{ij}^{\mathbf{E}}}{\kappa \kappa'}\right) & ((i, j) \in \mathcal{B}) \\ 0 & (\text{otherwise}) \end{cases}, \quad (13)$$

where $\tilde{T}_{ij}^{\mathbf{B}} \triangleq T_{ij}^{\mathbf{B}}(\tilde{\mathbf{Q}})$ and $\tilde{T}_{ij}^{\mathbf{E}} \triangleq T_{ij}^{\mathbf{E}}(\tilde{\mathbf{Q}})$ are defined according to Definition 18. Note that \mathbf{A} is a non-negative matrix, i.e., a matrix with non-negative entries. Let ρ be the Perron–Frobenius eigenvalue of the matrix \mathbf{A} , with corresponding right eigenvector $\boldsymbol{\gamma} = (\gamma_j)_{j \in \mathcal{S}}$.⁷ Define

$$\hat{p}_{ij}^* \triangleq \frac{A_{ij}}{\rho} \cdot \frac{\gamma_j}{\gamma_i}, \quad (i, j) \in \mathcal{B}. \quad (14)$$

Calculate $\{\hat{Q}_{ij}^*\}_{(i,j) \in \mathcal{B}}$ from $\{\hat{p}_{ij}^*\}_{(i,j) \in \mathcal{B}}$ (in the same way that we derived $\{Q_{ij}\}_{(i,j) \in \mathcal{B}}$ from $\{p_{ij}\}_{(i,j) \in \mathcal{B}}$). If

$$\kappa \geq \frac{\tilde{Q}_{ij} - \hat{Q}_{ij}^*}{\tilde{Q}_{ij}}, \quad (i, j) \in \mathcal{B}, \quad (15)$$

then the FSMS \mathbf{Q}^* is given by solving the system of linear equations

$$\begin{cases} Q_{ij}^* - \hat{p}_{ij}^* \sum_{j' \in \vec{\mathcal{S}}_i} Q_{ij'}^* - \frac{1-\kappa}{\kappa} \cdot (\tilde{\mu}_i \hat{p}_{ij}^* - \tilde{Q}_{ij}) = 0, & (i, j) \in \mathcal{B}, \\ \sum_{r \in \overleftarrow{\mathcal{S}}_i} Q_{ri}^* - \sum_{j \in \vec{\mathcal{S}}_i} Q_{ij}^* = 0, & i \in \mathcal{S}, \\ \sum_{(i,j) \in \mathcal{B}} Q_{ij}^* = 1, \end{cases}$$

in terms of $\{Q_{ij}^*\}_{(i,j) \in \mathcal{B}}$.

Proof. See Appendix D. □

Remark 29. Increasing the parameters κ and κ' has the effect of making the surrogate function narrower and steeper, implying a decreased step size.

Procedure 30. In the following, Algorithm 1 is leveraged to efficiently find an approximation $\check{\mathbf{Q}}^*$ to \mathbf{Q}^* by using the procedure in Proposition 28.⁸

⁷Recall that the Perron–Frobenius eigenvalue of a irreducible non-negative matrix is the eigenvalue with largest absolute value. One can show that the Perron–Frobenius eigenvalue is a positive real number and that the corresponding right eigenvector can be multiplied by a suitable scalar such that all entries are positive real numbers.

⁸The accuracy of the approximation can be controlled by choosing n suitably large.

- 1) Generate a sequence $\check{\mathbf{x}}_1^n$ based on the FSMS $\mathbf{Q} = \tilde{\mathbf{Q}}$.
- 2) Simulate Bob's (Eve's) channel with $\check{\mathbf{x}}_1^n$ at the input to obtain $\check{\mathbf{y}}_1^n$ ($\check{\mathbf{z}}_1^n$) at the output.
- 3) For every $(i, j) \in \mathcal{B}$, compute $\check{T}_{ij}^B(\tilde{\mathbf{Q}}, \check{\mathbf{y}}_1^n)$ and $\check{T}_{ij}^E(\tilde{\mathbf{Q}}, \check{\mathbf{z}}_1^n)$ according to (8) and (9).
- 4) Let $\check{\mathbf{A}} \triangleq (\check{A}_{ij})_{i,j \in \mathcal{S}}$ be the matrix with entries

$$\check{A}_{ij} \triangleq \begin{cases} \tilde{p}_{ij} \cdot \exp\left(\frac{\check{T}_{ij}^B(\tilde{\mathbf{Q}}, \check{\mathbf{y}}_1^n) - \check{T}_{ij}^E(\tilde{\mathbf{Q}}, \check{\mathbf{z}}_1^n)}{\kappa \kappa'}\right) & ((i, j) \in \mathcal{B}) \\ 0 & (\text{otherwise}) \end{cases}$$

- 5) Find the Perron–Frobenius eigenvalue $\check{\rho}$ and the corresponding right eigenvector $\check{\gamma}$ of the matrix $\check{\mathbf{A}}$.
- 6) Compute

$$\check{p}_{ij}^* \triangleq \frac{\check{A}_{ij}}{\check{\rho}} \cdot \frac{\check{\gamma}_j}{\check{\gamma}_i}, \quad (i, j) \in \mathcal{B}.$$

- 7) Calculate $\{\check{Q}_{ij}^*\}_{(i,j) \in \mathcal{B}}$ from $\{\check{p}_{ij}^*\}_{(i,j) \in \mathcal{B}}$ (in the same way that we derived $\{Q_{ij}\}_{(i,j) \in \mathcal{B}}$ from $\{p_{ij}\}_{(i,j) \in \mathcal{B}}$).
- 8) If $\kappa \geq (\tilde{Q}_{ij} - \check{Q}_{ij}^*)/\tilde{Q}_{ij}$, for all $(i, j) \in \mathcal{B}$, then the FSMS $\check{\mathbf{Q}}^*$ is given by solving the following system of linear equations in terms of $\{\check{Q}_{ij}^*\}_{(i,j) \in \mathcal{B}}$.

$$\begin{cases} \check{Q}_{ij}^* - \check{p}_{ij}^* \sum_{j' \in \vec{\mathcal{S}}_i} \check{Q}_{ij'}^* - \frac{1-\kappa}{\kappa} \cdot (\tilde{\mu}_i \check{p}_{ij}^* - \tilde{Q}_{ij}) = 0, & (i, j) \in \mathcal{B}, \\ \sum_{r \in \leftarrow \vec{\mathcal{S}}_i} \check{Q}_{ri}^* - \sum_{j \in \vec{\mathcal{S}}_i} \check{Q}_{ij}^* = 0, & i \in \mathcal{S}, \\ \sum_{(i,j) \in \mathcal{B}} \check{Q}_{ij}^* = 1. \end{cases}$$

- 9) Else, if $\kappa < (\tilde{Q}_{ij} - \check{Q}_{ij}^*)/\tilde{Q}_{ij}$, for any $(i, j) \in \mathcal{B}$, suitably change κ and go to step four.

Remark 31 (The EM Viewpoint). Procedure 30 can be considered as a variation of the well-known EM algorithm [39] comprised of two steps: Expectation (E-step) and Maximization (M-step). Namely, identifying a concave surrogate function around a local operating point resembles the E-step and maximization of the surrogate function to achieve a higher secure rate corresponds to the M-step (as summarized in Algorithm 2). Given this, the proposed algorithm has a similar convergence behavior (to a local maximum) as the EM algorithm [40].

Algorithm 2 Secure Rate Optimization

- 1: set $r \leftarrow 0$;
 - ▷ *Iteration* (until convergence)
 - 2: Apply Procedure 30 with input $\mathbf{Q} = \mathbf{Q}^{(r)}$ and output $\check{\mathbf{Q}}^*$
(suitably change the parameters κ, κ' if necessary);
 - 3: $r \leftarrow r + 1$;
 - 4: $\mathbf{Q}^{(r)} \leftarrow \check{\mathbf{Q}}^*$;
 - ◁ *End*
 - 5: Use Algorithm 1 with input $\mathbf{Q} = \mathbf{Q}^{(r)}$ and output \check{R}_s ;
 - 6: **return** \check{R}_s .
-

V. SIMULATION RESULTS AND DISCUSSION

In this section we apply the proposed algorithm, Algorithm 2, to two different ISI-WTCs and study the obtained achievable secure rates.

In previous sections, in order to keep the notation simple, we used the channel input alphabet $\mathcal{X} = \{+1, -1\}$ and unnormalized ISI channel transfer polynomials. However, in this section we use the channel input alphabet $\mathcal{X} = \{+\sqrt{E_s}, -\sqrt{E_s}\}$ and normalized ISI channel transfer polynomials, where a normalized transfer polynomial $g(D) \triangleq \sum_{t=0}^m g_t D^t \in \mathbb{R}[D]$ has to satisfy $\sum_{t=0}^m |g_t|^2 = 1$. (For a discussion on normalization of transfer polynomials, see, e.g., [41].)

A. Simulation Results

In general, we consider the following ISI-WTC setup:

- The transmitted symbols are BPSK modulated with the alphabet $\mathcal{X} = \{+\sqrt{E_s}, -\sqrt{E_s}\}$.
- Bob's channel is an ISI channel with normalized transfer polynomial $g^B(D)$ and additive white Gaussian noise of variance σ_B^2 .
- Eve's channel is an ISI channel with normalized transfer polynomial $g^E(D)$ and additive white Gaussian noise of variance σ_E^2 .
- The SNR of Bob's and Eve's channel is defined as $\text{SNR}^B \triangleq E_s/\sigma_B^2$ and $\text{SNR}^E \triangleq E_s/\sigma_E^2$, which in terms of decibels are $\text{SNR}_{\text{dB}}^B \triangleq 10 \log_{10}(E_s/\sigma_B^2)$ and $\text{SNR}_{\text{dB}}^E \triangleq 10 \log_{10}(E_s/\sigma_E^2)$, respectively.⁹

⁹If desired, these SNR values can be re-expressed in terms of E_s/N_0 values, where N_0 is the two-sided power spectral density of the AWGN process: $E_s/N_0 = \frac{1}{2} \cdot (E_s/\sigma^2)$.

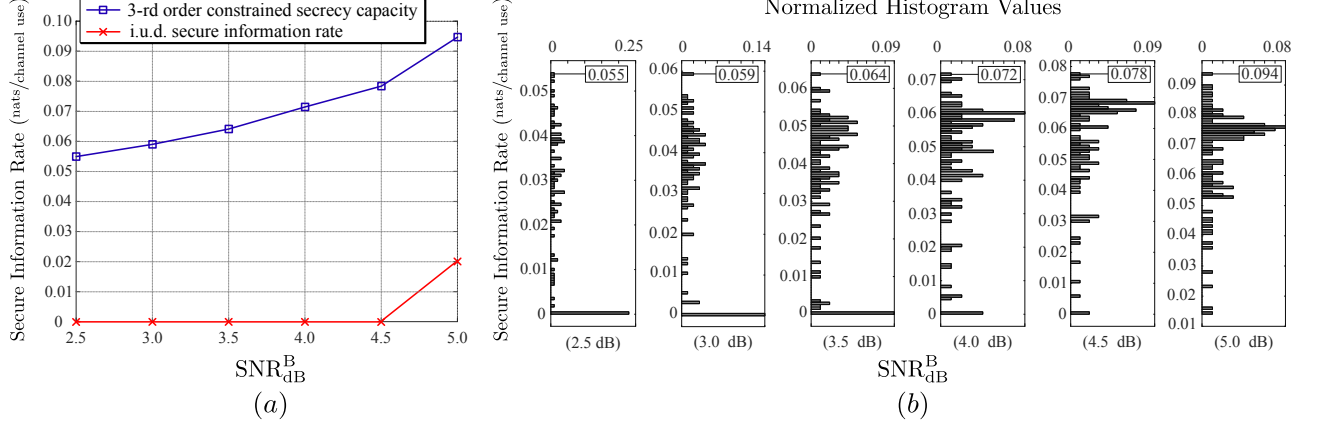


Fig. 4: Simulation results for the setup in Example 32. (a) The 3rd order constrained secrecy capacity and the secure rates of an i.u.d. input process when $\text{SNR}_{\text{dB}}^{\text{E}} = 5.0$ dB. (b) Normalized histogram functions of the locally-optimum secure rates obtained from running Algorithm 2 with 100 different initializations.

Example 32. We consider the following setup:

- An FSMS as in Remark 2 with $\bar{\nu} = 3$.
- Bob's channel is a decode channel, i.e., $g^{\text{B}}(D) = \frac{1}{\sqrt{2}} \cdot (1 - D)$.
- Eve's channel is an EPR4 channel, i.e., $g^{\text{E}}(D) = \frac{1}{2} \cdot (1 + D - D^2 - D^3)$.

Fig. 4(a) shows the obtained secure information rates: on the one hand for an *unoptimized* FSMS, i.e., an FSMS producing i.u.d. symbols, and, on the other hand, for an *optimized* FSMS, where the optimization was done with the help of Algorithm 2. In this plot, for every $\text{SNR}_{\text{dB}}^{\text{B}}$ value, the best obtained secure information rate is plotted after running Algorithm 2 for 100 different initializations.¹⁰ In fact, it is important to run Algorithm 2 with several initializations because the secure information rate is a highly fluctuating function, which is witnessed by the broad histograms in Fig. 4(b) that show the obtained secure information rates for various initializations of Algorithm 2.

Example 33. We consider the following setup:

- An FSMS as in Remark 2 with $\bar{\nu} = 3$.
- Bob's channel is an EPR4 channel, i.e., $g^{\text{B}}(D) = \frac{1}{2} \cdot (1 + D - D^2 - D^3)$.
- Eve's channel is a decode channel, i.e., $g^{\text{E}}(D) = \frac{1}{\sqrt{2}} \cdot (1 - D)$.

The obtained results are shown in Figs. 5(a) and (b). (These figures are similar to Figs. 4(a) and (b) for Example 32.)

¹⁰These initializations were generated with the help of Weyl's $|\mathcal{S}|$ -dimensional equi-distributed sequences [42].

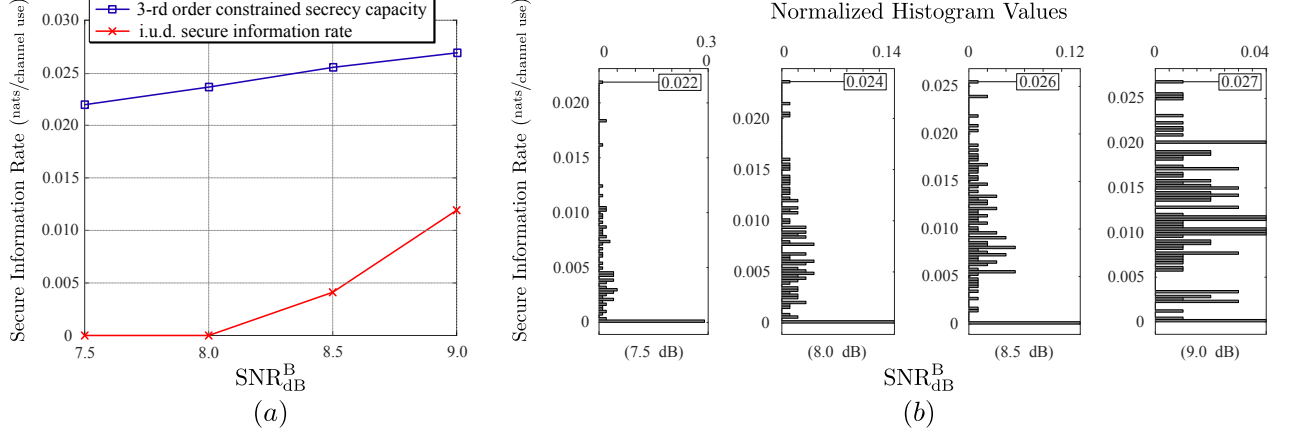


Fig. 5: Simulation results for the setup in Example 33. (a) The 3rd order constrained secrecy capacity and the secure rates of an i.u.d. input process when $\text{SNR}_{\text{dB}}^{\text{E}} = 8.0$ dB. (b) Normalized histogram functions of the locally-optimum secure rates obtained from running Algorithm 2 with 100 different initializations.

Note that when running Algorithm 2, we used κ and κ' values in the ranges $0.8 \leq \kappa \leq 1$ and $5 \leq \kappa' \leq 10$, respectively. Typically, 30 to 40 iterations were needed to reach numerical convergence.

B. Discussion

As we have seen in Section V-A, positive secure information rates are possible and optimizing the FSMS clearly benefits these rates. Interestingly, positive secure information rates are also possible when the point-to-point channel to Eve is “better” than the point-to-point channel to Bob. In order to make this discussion more insightful and analytically tractable, we consider in this section the scenario where the only channel input constraint is an average energy constraint. This allows us to use Fourier transform techniques and well-known “water-pouring” formulas for analyzing capacities of such point-to-point channels.

Namely, consider an ISI channel described by the transfer polynomial $g(D) = \sum_{t=0}^m g_t D^t$ and with additive (possibly non-white) Gaussian noise. The unconstrained (besides some average-energy constraint) capacity of this channel is given by the “water-pouring” formula (see, e.g., [41])

$$C = \frac{1}{2} \cdot \int_{-\infty}^{\infty} \max \left\{ 0, \log \left(\frac{\alpha}{N(f)/|G(f)|^2} \right) \right\} df,$$

where

$$G(f) = \begin{cases} \frac{\sum_{\ell=0}^m g_{\ell} e^{-j2\ell\pi fT}}{\sum_{\ell=0}^m |g_{\ell}|^2} & (\text{if } |f| \leq W) \\ 0 & (\text{otherwise}) \end{cases},$$

and where $\alpha > 0$ is chosen such that

$$E_s = \int_{-\infty}^{\infty} \max \left\{ 0, \alpha - \frac{N(f)}{|G(f)|^2} \right\} df.$$

This capacity formula is based on the following assumptions:

- average energy constraint per input symbol E_s ;
- symbol period T (in seconds);
- a perfect lowpass filter of bandwidth $W \triangleq \frac{1}{2T}$ and sampling at the Nyquist frequency $1/T$ at the receiver side;
- power spectral density $N(f)$ (in Watts per Hertz) of the additive Gaussian noise before the lowpass filter.

The resulting unconstrained capacities for a dicode and an EPR4 channel are shown in Fig. 6 and Fig. 7.

Example 34 (Continuation of Example 32). Consider the scenario where $E_s = 1$ J, $2.5 \text{ dB} \leq \text{SNR}_{\text{dB}}^{\text{B}} \leq 5 \text{ dB}$, and $\text{SNR}_{\text{dB}}^{\text{E}} = 5 \text{ dB}$. It can be seen from Fig. 6 that Eve's channel has a higher unconstrained capacity than Bob's channel for sufficiently large enough bandwidth. In this sense, Bob's channel is “worse” than Eve's channel. However, luckily for Bob, there are frequencies where Bob's channel has a better gain-to-noise spectrum ratio than Eve's channel, as can be seen from Fig. 8(a). This can be exploited by a suitably tuned source at the channel input toward obtaining positive secure information rates.

Example 35 (Continuation of Example 33). Consider the scenario where $E_s = 1$ J, $7.5 \text{ dB} \leq \text{SNR}_{\text{dB}}^{\text{B}} \leq 9 \text{ dB}$, and $\text{SNR}_{\text{dB}}^{\text{E}} = 8 \text{ dB}$. It can be seen from Fig. 7 that Bob's channel has a higher unconstrained capacity than Eve's channel for sufficiently large enough bandwidth. In this sense, it is not unexpected that positive secure information rates are possible. Nevertheless, it is worthwhile to point out that here secure information rates are possible even though Bob's channel has larger memory and, for some selections of $\text{SNR}_{\text{dB}}^{\text{B}}$, higher

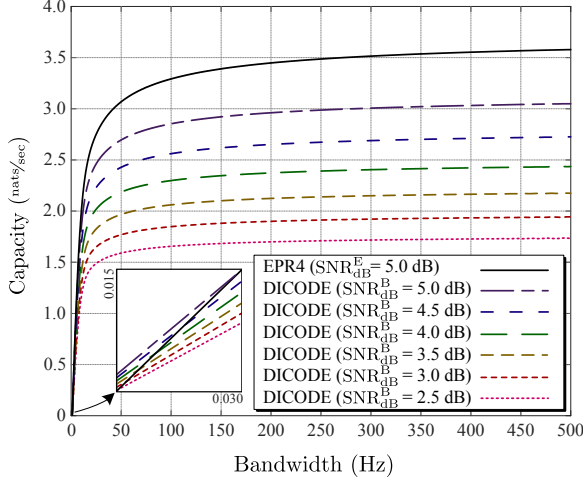


Fig. 6: Capacity of the dicode and the EPR4 channels in nats/sec with input power $E_s = 1$ J, for the SNR values corresponding to Example 32.

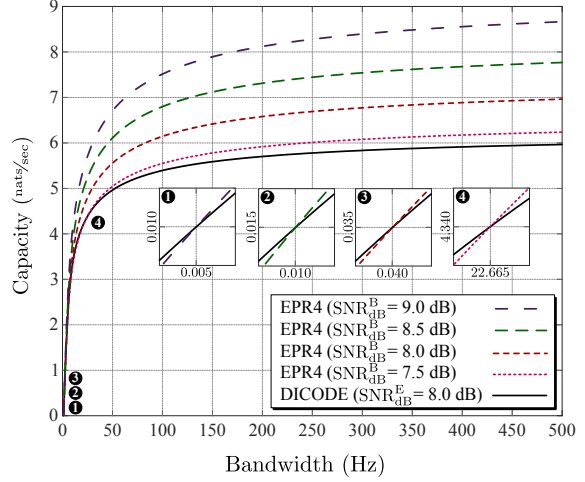


Fig. 7: Capacity of the dicode and the EPR4 channels in nats/sec with input power $E_s = 1$ J, for the SNR values corresponding to Example 33.

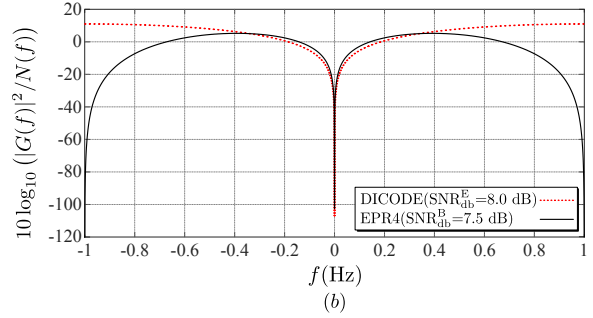
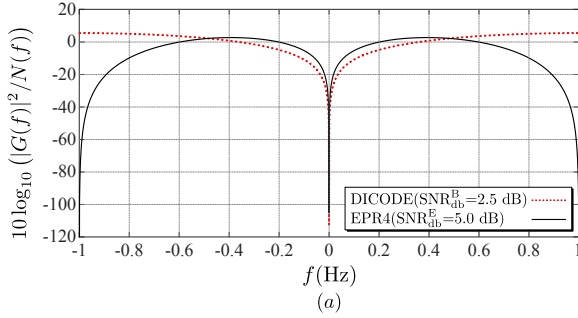


Fig. 8: The channel's gain-to-noise spectrum ratio in decibels per frequency (Hz) corresponding to Examples 32 and 33.

noise power than Eve's channel (see Fig. 8(b)).

In a conventional DM-WTC [29], [31], Eve's channel necessarily has to be noisier than Bob's channel in order to achieve a positive secrecy capacity. This results in the capacity of Eve's channel to be less than the capacity of Bob's channel. In contrast, we showed that positive secure information rates are achievable on the ISI-WTCs, even if

- the unconstrained capacity of Bob's channel is smaller than the unconstrained capacity of Eve's channel (Example 32);
- Bob's channel tolerates both a higher noise power and a larger memory compared with Eve's channel (Example 33).

VI. CONCLUSION

In this paper, we have optimized an FSMS at the input of an ISI-WTC toward (locally) maximizing the secrecy rate. Because directly maximizing the secrecy rate function is challenging, we have iteratively approximated the secrecy rate function by a surrogate function whose maximum can be found efficiently.

Our numerical results show that by implicitly using the discrepancies between the frequency responses of Bob's and Eve's channels, it is possible to achieve positive secrecy rates also for setups where the unconstrained capacity of Eve's channel is larger than the unconstrained capacity of Bob's channel.

APPENDIX A

PROOF OF PROPOSITION 14

Let $\{\mathbf{X}_{k(\ell+2\nu)-\nu+1}^{k(\ell+2\nu)+(\ell+\nu)}\}_{k=-\infty}^{+\infty}$ be a block i.i.d. process where each block has length $\ell + 2\nu$. It suffices to specify the distribution of a single block $\mathbf{X}_{k(\ell+2\nu)-\nu+1}^{k(\ell+2\nu)+(\ell+\nu)}$. In order to ensure that there is no interference across blocks, we set

$$X_{k(\ell+2\nu)+(\ell+1)} \triangleq 0, \quad \dots, \quad X_{k(\ell+2\nu)+(\ell+\nu)} \triangleq 0,$$

while allowing $\mathbf{X}_{k(\ell+2\nu)-\nu+1}^{k(\ell+2\nu)+\ell}$ to be arbitrarily distributed. It is easy to verify that

$$\left\{ \mathbf{X}_{k(\ell+2\nu)-\nu+1}^{k(\ell+2\nu)+(\ell+\nu)}, \mathbf{Y}_{k(\ell+2\nu)-\nu+1}^{k(\ell+2\nu)+(\ell+\nu)} \right\}_{k=-\infty}^{+\infty}$$

is a joint block i.i.d. process. Similarly,

$$\left\{ \mathbf{X}_{k(\ell+2\nu)-\nu+1}^{k(\ell+2\nu)+(\ell+\nu)}, \mathbf{Z}_{k(\ell+2\nu)-\nu+1}^{k(\ell+2\nu)+(\ell+\nu)} \right\}_{k=-\infty}^{+\infty}$$

is also a joint block i.i.d. processes. It follows by the strong law of large numbers that

$$\begin{aligned} \lim_{n \rightarrow \infty} \frac{1}{n} i(\mathbf{X}_1^n; \mathbf{Y}_1^n) &= \frac{1}{\ell + 2\nu} I(\mathbf{X}_{-\nu+1}^{\ell+\nu}; \mathbf{Y}_{-\nu+1}^{\ell+\nu}) \quad \text{w.p. 1,} \\ \lim_{n \rightarrow \infty} \frac{1}{n} i(\mathbf{X}_1^n; \mathbf{Z}_1^n) &= \frac{1}{\ell + 2\nu} I(\mathbf{X}_{-\nu+1}^{\ell+\nu}; \mathbf{Z}_{-\nu+1}^{\ell+\nu}) \quad \text{w.p. 1.} \end{aligned}$$

Note that,

$$I(\mathbf{X}_{-\nu+1}^{\ell+\nu}; \mathbf{Y}_{-\nu+1}^{\ell+\nu}) \geq I(\mathbf{X}_{-\nu+1}^{\ell}; \mathbf{Y}_1^{\ell}) = I(\mathbf{X}_{-\nu+1}^0; \mathbf{Y}_1^{\ell}) + I(\mathbf{X}_1^{\ell}; \mathbf{Y}_1^{\ell} | \mathbf{X}_{-\nu+1}^0) \geq I(\mathbf{X}_1^{\ell}; \mathbf{Y}_1^{\ell} | \mathbf{X}_{-\nu+1}^0).$$

Moreover,

$$\begin{aligned}
I(\mathbf{X}_{-\nu+1}^{\ell+\nu}; \mathbf{Z}_{-\nu+1}^{\ell+\nu}) &= I(\mathbf{X}_{-\nu+1}^{\ell}; \mathbf{Z}_{-\nu+1}^{\ell+\nu}) \\
&= I(\mathbf{X}_{-\nu+1}^{\ell}; \mathbf{Z}_1^{\ell}) + I(\mathbf{X}_{-\nu+1}^{\ell}; \mathbf{Z}_{-\nu+1}^0 | \mathbf{Z}_1^{\ell}) + I(\mathbf{X}_{-\nu+1}^{\ell}; \mathbf{Z}_{\ell+1}^{\ell+\nu} | \mathbf{Z}_{-\nu+1}^{\ell}) \\
&= I(\mathbf{X}_1^{\ell}; \mathbf{Z}_1^{\ell} | \mathbf{X}_{-\nu+1}^0) + I(\mathbf{X}_{-\nu+1}^0; \mathbf{Z}_1^{\ell}) + I(\mathbf{X}_{-\nu+1}^{\ell}; \mathbf{Z}_{-\nu+1}^0 | \mathbf{Z}_1^{\ell}) + I(\mathbf{X}_{-\nu+1}^{\ell}; \mathbf{Z}_{\ell+1}^{\ell+\nu} | \mathbf{Z}_{-\nu+1}^{\ell}) \\
&= I(\mathbf{X}_1^{\ell}; \mathbf{Z}_1^{\ell} | \mathbf{X}_{-\nu+1}^0) + I(\mathbf{X}_{-\nu+1}^0; \mathbf{Z}_1^{\ell}) + I(\mathbf{X}_{-\nu+1}^0; \mathbf{Z}_{-\nu+1}^0 | \mathbf{Z}_1^{\ell}) + I(\mathbf{X}_{-\nu+1}^{\ell}; \mathbf{Z}_{\ell+1}^{\ell+\nu} | \mathbf{Z}_{-\nu+1}^{\ell}) \\
&\leq I(\mathbf{X}_1^{\ell}; \mathbf{Z}_1^{\ell} | \mathbf{X}_{-\nu+1}^0) + 3\nu \log |\mathcal{X}|.
\end{aligned}$$

Combining Lemma 13 with the above lower and upper bounds concludes the proof.

APPENDIX B

PROOF OF PROPOSITION 19

Reformulating the expression in (5), we obtain

$$\begin{aligned}
R_s &= \lim_{n \rightarrow \infty} \frac{1}{n} \left(I(\mathbf{S}_1^n; \mathbf{Y}_1^n | S_0) - I(\mathbf{S}_1^n; \mathbf{Z}_1^n | S_0) \right) = \lim_{n \rightarrow \infty} \frac{1}{n} \sum_{t=1}^n \left(I(S_t; \mathbf{Y}_1^n | S_0^{t-1}) - I(S_t; \mathbf{Z}_1^n | S_0^{t-1}) \right) \\
&= \lim_{n \rightarrow \infty} \frac{1}{n} \sum_{t=1}^n \left(I(S_t; \mathbf{Y}_1^n | S_{t-1}) - I(S_t; \mathbf{Z}_1^n | S_{t-1}) \right) = \lim_{n \rightarrow \infty} \frac{1}{n} \sum_{t=1}^n \left(H(S_t | \mathbf{Z}_1^n, S_{t-1}) - H(S_t | \mathbf{Y}_1^n, S_{t-1}) \right) \\
&= \sum_{(i,j) \in \mathcal{B}} Q_{ij} \cdot (T_{ij}^B(\mathbf{Q}) - T_{ij}^E(\mathbf{Q})),
\end{aligned}$$

where the last equality is based on expressing $H(S_t | \mathbf{Y}_1^n, S_{t-1})$ as

$$\begin{aligned}
H(S_t | \mathbf{Y}_1^n, S_{t-1}) &= - \sum_{(i,j) \in \mathcal{B}} \int_{\mathbf{y}_1^n \in \mathcal{Y}^n} p_{S_t, S_{t-1}, \mathbf{Y}_1^n}(j, i, \mathbf{y}_1^n) \cdot \log(p_{S_t | S_{t-1}, \mathbf{Y}_1^n}(j | i, \mathbf{y}_1^n)) d\mathbf{y}_1^n \\
&= - \sum_{(i,j) \in \mathcal{B}} \int_{\mathbf{y}_1^n \in \mathcal{Y}^n} p_{S_t, S_{t-1}, \mathbf{Y}_1^n}(j, i, \mathbf{y}_1^n) \cdot \left(\log \left(\frac{p_{S_t, S_{t-1}, \mathbf{Y}_1^n}(j, i, \mathbf{y}_1^n)}{p_{\mathbf{Y}_1^n}(\mathbf{y}_1^n)} \right) - \log \left(\frac{p_{S_{t-1}, \mathbf{Y}_1^n}(i, \mathbf{y}_1^n)}{p_{\mathbf{Y}_1^n}(\mathbf{y}_1^n)} \right) \right) d\mathbf{y}_1^n \\
&= - \sum_{(i,j) \in \mathcal{B}} \mu_i p_{ij} \cdot \int_{\mathbf{y}_1^n \in \mathcal{Y}^n} \left(p_{\mathbf{Y}_1^n | S_{t-1}, S_t}(\mathbf{y}_1^n | i, j) \cdot \log(p_{S_{t-1}, S_t | \mathbf{Y}_1^n}(i, j | \mathbf{y}_1^n)) \right. \\
&\quad \left. - p_{\mathbf{Y}_1^n | S_{t-1}}(\mathbf{y}_1^n | i) \cdot \log(p_{S_{t-1} | \mathbf{Y}_1^n}(i | \mathbf{y}_1^n)) \right) d\mathbf{y}_1^n \\
&= - \sum_{(i,j) \in \mathcal{B}} \mu_i p_{ij} \cdot \int_{\mathbf{y}_1^n \in \mathcal{Y}^n} \left(\frac{p_{S_{t-1}, S_t | \mathbf{Y}_1^n}(i, j | \mathbf{y}_1^n)}{\mu_i p_{ij}} \cdot p_{\mathbf{Y}_1^n}(\mathbf{y}_1^n) \cdot \log(p_{S_{t-1}, S_t | \mathbf{Y}_1^n}(i, j | \mathbf{y}_1^n)) \right. \\
&\quad \left. - \frac{p_{S_{t-1} | \mathbf{Y}_1^n}(i | \mathbf{y}_1^n)}{\mu_i} \cdot p_{\mathbf{Y}_1^n}(\mathbf{y}_1^n) \cdot \log(p_{S_{t-1} | \mathbf{Y}_1^n}(i | \mathbf{y}_1^n)) \right) d\mathbf{y}_1^n \\
&= - \sum_{(i,j) \in \mathcal{B}} \mu_i p_{ij} \cdot \left(\int_{\mathbf{y}_1^n \in \mathcal{Y}^n} p_{\mathbf{Y}_1^n}(\mathbf{y}_1^n) \cdot \log \left(\frac{p_{S_{t-1}, S_t | \mathbf{Y}_1^n}(i, j | \mathbf{y}_1^n)^{p_{S_{t-1}, S_t | \mathbf{Y}_1^n}(i, j | \mathbf{y}_1^n) / \mu_i p_{ij}}}{p_{S_{t-1} | \mathbf{Y}_1^n}(i | \mathbf{y}_1^n)^{p_{S_{t-1} | \mathbf{Y}_1^n}(i | \mathbf{y}_1^n) / \mu_i}} \right) d\mathbf{y}_1^n \right)
\end{aligned}$$

with an analogous expression for $H(S_t|\mathbf{Z}_1^n, S_{t-1})$, along with using (6) and (7).

APPENDIX C

PROOF OF LEMMA 26

Besides the assumptions on the parameterizations $\mathbf{Q}(\theta)$ made in Assumption 22, we will also assume that for all $(i, j) \in \mathcal{B}$, the functions $Q_{ij}(\theta)$ and $\mu_i(\theta)$ are affine functions of θ , which implies that

$$Q_{ij}^{\theta\theta}(\theta) = 0, \quad \mu_i^{\theta\theta}(\theta) = 0,$$

where the superscript $\theta\theta$ denotes the second-order derivative w.r.t. θ .

Denoting the second-order derivative of $\bar{\psi}_{\mathbf{Q}}(\theta)$ by $\bar{\psi}_{\mathbf{Q}}^{\theta\theta}(\theta)$, we observe that the claim in the lemma statement is equivalent to $\bar{\psi}_{\mathbf{Q}}^{\theta\theta}(\theta) \geq 0$ for all possible parameterizations of $\mathbf{Q}(\theta)$ that satisfy the above-mentioned conditions.

Some straightforward calculations show that

$$\bar{\psi}_{\mathbf{Q}}^{\theta\theta}(\theta) = \kappa^2 \kappa' \cdot \left(\sum_{(i,j) \in \mathcal{B}} \frac{(Q_{ij}^\theta)^2}{Q_{ij}} - \sum_{i \in \mathcal{S}} \frac{(\mu_i^\theta)^2}{\mu_i} \right) = \kappa^2 \kappa' \cdot \sum_{i \in \mathcal{S}} \left(\left(\sum_{j \in \vec{\mathcal{S}}_i} \frac{(Q_{ij}^\theta)^2}{Q_{ij}} \right) - \frac{(\mu_i^\theta)^2}{\mu_i} \right).$$

Noting that for any $i \in \mathcal{S}$ it holds that

$$\sum_{j \in \vec{\mathcal{S}}_i} \frac{(Q_{ij}^\theta)^2}{Q_{ij}} = \mu_i \cdot \sum_{j \in \vec{\mathcal{S}}_i} \frac{Q_{ij}}{\mu_i} \cdot \left(\frac{Q_{ij}^\theta}{Q_{ij}} \right)^2 \geq \mu_i \cdot \left(\sum_{j \in \vec{\mathcal{S}}_i} \frac{Q_{ij}}{\mu_i} \cdot \frac{Q_{ij}^\theta}{Q_{ij}} \right)^2 = \frac{1}{\mu_i} \cdot \left(\sum_{j \in \vec{\mathcal{S}}_i} Q_{ij}^\theta \right)^2 = \frac{(\mu_i^\theta)^2}{\mu_i},$$

where the inequality follows from Jensen's inequality. Combining the above two display equations, we can conclude that, indeed, $\bar{\psi}_{\mathbf{Q}}^{\theta\theta}(\theta) \geq 0$.

APPENDIX D

PROOF OF PROPOSITION 28

Maximizing $\psi_{\mathbf{Q}}(\mathbf{Q})$ over $\mathbf{Q} \in \mathcal{Q}(\mathcal{B})$ means to optimize a differentiable, concave function over a polytope. We therefore set up the Lagrangian

$$L \triangleq \sum_{(i,j) \in \mathcal{B}} Q_{ij} \cdot (\tilde{T}_{ij}^{\text{B}} - \tilde{T}_{ij}^{\text{E}}) - \bar{\psi}_{\mathbf{Q}}(\mathbf{Q}) + \lambda \cdot \left(\sum_{(i,j) \in \mathcal{B}} Q_{ij} - 1 \right) + \sum_{(i,j) \in \mathcal{B}} \lambda_j Q_{ij} - \sum_{(i,j) \in \mathcal{B}} \lambda_i Q_{ij}.$$

Note that at this stage we omit Lagrangian multipliers w.r.t. the constraints $Q_{ij} \geq 0$, $(i, j) \in \mathcal{B}$. We will make sure at a later stage that these constraints are satisfied thanks to the choice of κ in (15).

Recall that we assume that the surrogate function takes on its maximal value at $\mathbf{Q} = \mathbf{Q}^*$. Therefore, setting the gradient of L equal to the zero vector at $\mathbf{Q} = \mathbf{Q}^*$, we obtain

$$\begin{aligned} 0 &= \left. \frac{\partial L}{\partial Q_{ij}} \right|_{\mathbf{Q}=\mathbf{Q}^*} = \tilde{T}_{ij}^B - \tilde{T}_{ij}^E - \left. \frac{\partial \bar{\psi}_{\tilde{\mathbf{Q}}}(\mathbf{Q})}{\partial Q_{ij}} \right|_{\mathbf{Q}=\mathbf{Q}^*} + \lambda^* + \lambda_j^* - \lambda_i^*, \quad (i, j) \in \mathcal{B}, \\ 0 &= \left. \frac{\partial L}{\partial \lambda} \right|_{\mathbf{Q}=\mathbf{Q}^*} = \sum_{(i,j) \in \mathcal{B}} Q_{ij}^* - 1, \\ 0 &= \left. \frac{\partial L}{\partial \lambda_i} \right|_{\mathbf{Q}=\mathbf{Q}^*} = \sum_{r \in \overleftarrow{\mathcal{S}}_i} Q_{ri}^* - \sum_{j \in \overrightarrow{\mathcal{S}}_i} Q_{ij}^*, \quad i \in \mathcal{S}, \end{aligned} \quad (16)$$

where

$$\begin{aligned} \left. \frac{\partial \bar{\psi}_{\tilde{\mathbf{Q}}}(\mathbf{Q})}{\partial Q_{ij}} \right|_{\mathbf{Q}=\mathbf{Q}^*} &= \kappa' \cdot \left(\kappa \cdot \log(1 + \kappa \cdot (\delta Q)_{ij}) - \kappa \cdot \log(1 + \kappa \cdot (\delta \mu)_i) \right) \Big|_{\mathbf{Q}=\mathbf{Q}^*} \\ &= \kappa \cdot \kappa' \cdot \log \left(\frac{(1 - \kappa) \cdot \tilde{Q}_{ij} + \kappa \cdot Q_{ij}^*}{(1 - \kappa) \cdot \tilde{\mu}_i + \kappa \cdot \mu_i^*} \cdot \frac{\tilde{\mu}_i}{\tilde{Q}_{ij}} \right) \\ &= \kappa \cdot \kappa' \cdot \log \left(\frac{\hat{Q}_{ij}^*}{\hat{\mu}_i^*} \cdot \frac{\tilde{\mu}_i}{\tilde{Q}_{ij}} \right) = \kappa \cdot \kappa' \cdot \log(\hat{p}_{ij}^*) - \kappa \cdot \kappa' \cdot \log(\tilde{p}_{ij}). \end{aligned} \quad (17)$$

Here the third and fourth equality use $\{\hat{Q}_{ij}^*\}_{(i,j) \in \mathcal{B}}$, which is defined by

$$\hat{Q}_{ij}^* \triangleq (1 - \kappa) \cdot \tilde{Q}_{ij} + \kappa \cdot Q_{ij}^*, \quad (i, j) \in \mathcal{B}, \quad (18)$$

along with $\{\hat{\mu}_i^*\}_{i \in \mathcal{S}}$ and $\{\hat{p}_{ij}^*\}_{(i,j) \in \mathcal{B}}$, which are derived from $\{\hat{Q}_{ij}^*\}_{(i,j) \in \mathcal{B}}$ in the usual manner.

Note that $\hat{\mu}_i^* = (1 - \kappa) \cdot \tilde{\mu}_i + \kappa \cdot \mu_i^*$, for all $i \in \mathcal{S}$, and

$$\hat{p}_{ij}^* = \frac{\hat{Q}_{ij}^*}{\hat{\mu}_i^*} = \frac{(1 - \kappa) \cdot \tilde{Q}_{ij} + \kappa \cdot Q_{ij}^*}{(1 - \kappa) \cdot \tilde{\mu}_i + \kappa \cdot \mu_i^*} = \frac{(1 - \kappa) \cdot \tilde{Q}_{ij} + \kappa \cdot Q_{ij}^*}{(1 - \kappa) \cdot \tilde{\mu}_i + \kappa \cdot \sum_{j' \in \overrightarrow{\mathcal{S}}_i} Q_{ij'}^*}, \quad (i, j) \in \mathcal{B}. \quad (19)$$

Note also that solving (18) for Q_{ij}^* results in

$$Q_{ij}^* = \frac{1}{\kappa} \cdot (\hat{Q}_{ij}^* - \tilde{Q}_{ij} + \kappa \cdot \tilde{Q}_{ij}), \quad (i, j) \in \mathcal{B},$$

which shows that $Q_{ij}^* \geq 0$, $(i, j) \in \mathcal{B}$, for κ satisfying (15). (Recall that when setting up

the Lagrangian, we omitted the Lagrange multipliers for the constraints $Q_{ij} \geq 0$, $(i, j) \in \mathcal{B}$; therefore we have to verify that the solution satisfies these constraints, which it does indeed.)

Combining (16) and (17) and solving for \hat{p}_{ij}^* results in

$$\hat{p}_{ij}^* = \tilde{p}_{ij} \cdot \exp\left(\frac{\tilde{T}_{ij}^B - \tilde{T}_{ij}^E + \lambda^* + \lambda_j^* - \lambda_i^*}{\kappa\kappa'}\right), \quad (i, j) \in \mathcal{B}.$$

Using (13) and defining $\rho \triangleq \exp\left(-\frac{\lambda^*}{\kappa\kappa'}\right)$ and $\boldsymbol{\gamma} = (\gamma_i)_{i \in \mathcal{S}}$, where $\gamma_i \triangleq \exp\left(\frac{\lambda_i^*}{\kappa\kappa'}\right)$, allows the rewriting of this equation as

$$\hat{p}_{ij}^* = \frac{A_{ij}}{\rho} \cdot \frac{\gamma_j}{\gamma_i}, \quad (i, j) \in \mathcal{B}.$$

Because $\sum_{j \in \vec{\mathcal{S}}_i} \hat{p}_{ij}^* = 1$ for all $i \in \mathcal{S}$, summing both sides of this equation over $j \in \vec{\mathcal{S}}_i$ results in

$$1 = \sum_{j \in \vec{\mathcal{S}}_i} \frac{A_{ij}}{\rho} \cdot \frac{\gamma_j}{\gamma_i}, \quad i \in \mathcal{S},$$

or, equivalently,

$$\rho \cdot \gamma_i = \sum_{j \in \vec{\mathcal{S}}_i} A_{ij} \cdot \gamma_j, \quad i \in \mathcal{S}.$$

This system of linear equations can be written as

$$\mathbf{A} \cdot \boldsymbol{\gamma} = \rho \cdot \boldsymbol{\gamma}.$$

Clearly, this equation can only be satisfied if $\boldsymbol{\gamma}$ is an eigenvector of \mathbf{A} with corresponding eigenvalue ρ . A slightly lengthy calculation (which is somewhat similar to the calculation in [17, Eq. (51)]) shows that

$$\psi_{\tilde{\mathbf{Q}}}(\mathbf{Q}^*) = \log(\rho).$$

As is well known, Perron–Frobenius theory guarantees for an irreducible non-negative matrix that the eigenvalue with largest absolute value is a positive real number, called the Perron–Frobenius eigenvalue. Therefore, in order to maximize $\log(\rho)$ over all eigenvalues of \mathbf{A} , the eigenvalue ρ has to be the Perron–Frobenius eigenvalue and $\boldsymbol{\gamma}$ the corresponding eigenvector.

The proof is concluded by noting that (19) can be rewritten as the system of linear equations

$$Q_{ij}^* - \hat{p}_{ij}^* \cdot \sum_{j' \in \vec{\mathcal{S}}_i} Q_{ij'}^* = \frac{1 - \kappa}{\kappa} \cdot (\tilde{\mu}_i \hat{p}_{ij}^* - \tilde{Q}_{ij}), \quad (i, j) \in \mathcal{B},$$

which can be used to determine $\{Q_{ij}^*\}_{(i,j) \in \mathcal{B}}$, because all other quantities appearing in these equations are either known or have already been calculated.

REFERENCES

- [1] Y. Liu, H. H. Chen, and L. Wang, “Physical layer security for next generation wireless networks: Theories, technologies, and challenges,” *IEEE Commun. Surv. Tutor.*, vol. 19, no. 1, pp. 347–376, 2017.
- [2] C. Gidney and M. Ekerå, “How to factor 2048 bit RSA integers in 8 hours using 20 million noisy qubits,” *Quantum*, vol. 5, p. 433, Apr. 2021.
- [3] M. Bloch, O. Günlü, A. Yener, F. Oggier, H. V. Poor, L. Sankar, and R. F. Schaefer, “An overview of information-theoretic security and privacy: Metrics, limits and applications,” *IEEE J. Sel. Areas Inf. Theory*, vol. 2, no. 1, pp. 5–22, Mar. 2021.
- [4] J. M. Hamamreh, H. M. Furqan, and H. Arslan, “Classifications and applications of physical layer security techniques for confidentiality: A comprehensive survey,” *IEEE Commun. Surv. Tutor.*, vol. 21, no. 2, pp. 1773–1828, 2019.
- [5] J. G. Proakis and M. Salehi, *Digital communications 5th edition*. McGraw Hill, 2008.
- [6] European Telecommunications Standards Institute, “Evolved universal terrestrial radio access (E-UTRAN): Physical channels and modulation,” *ETSI TS 136 211 V14.2.0*, Apr. 2017.
- [7] C. Kuhfins, B. Rathonyi, A. Zaidi, and M. Hogan, “Cellular networks for massive IoT,” *Ericsson White Paper Uen 284 23-3278*, Jan. 2020.
- [8] Y. Cao, W. Shi, L. Sun, and X. Fu, “Channel state information-based ranging for underwater acoustic sensor networks,” *IEEE Trans. Wirel. Commun.*, vol. 20, no. 2, pp. 1293–1307, Feb. 2021.
- [9] B. Dai, Z. Ma, Y. Luo, X. Liu, Z. Zhuang, and M. Xiao, “Enhancing physical layer security in internet of things via feedback: A general framework,” *IEEE Internet Things J.*, vol. 7, no. 1, pp. 99–115, Oct. 2020.
- [10] J. Zhang, S. Rajendran, Z. Sun, R. Woods, and L. Hanzo, “Physical layer security for the internet of things: Authentication and key generation,” *IEEE Wirel. Commun.*, vol. 26, no. 5, pp. 92–98, May 2019.
- [11] S. Jiang, “On securing underwater acoustic networks: A survey,” *IEEE Commun. Surv. Tutor.*, vol. 21, no. 1, pp. 729–752, Aug. 2019.
- [12] 5G Americas White Paper, “Understanding mmWave spectrum for 5G networks,” *5G Americas*, Dec. 2020.
- [13] K. Aldubaikhy, W. Wu, N. Zhang, N. Cheng, and X. Shen, “mmWave IEEE 802.11ay for 5G fixed wireless access,” *IEEE Wirel. Commun.*, vol. 27, no. 2, pp. 88–95, Apr. 2020.
- [14] R. G. Gallager, *Information Theory and Reliable Communication*. New York, NY, USA: John Wiley & Sons, 1968.
- [15] R. Blahut, “Computation of channel capacity and rate-distortion functions,” *IEEE Trans. Inf. Theory*, vol. 18, no. 4, pp. 460–473, July 1972.
- [16] S. Arimoto, “An algorithm for computing the capacity of arbitrary discrete memoryless channels,” *IEEE Trans. Inf. Theory*, vol. 18, no. 1, pp. 14–20, Jan. 1972.
- [17] P. O. Vontobel, A. Kavčić, D. M. Arnold, and H.-A. Loeliger, “A generalization of the Blahut-Arimoto algorithm to finite-state channels,” *IEEE Trans. Inf. Theory*, vol. 54, no. 5, pp. 1887–1918, May 2008.
- [18] A. Kavčić, “On the capacity of Markov sources over noisy channels,” in *Proc. IEEE Global Communications Conference*, vol. 5, San Antonio, TX, USA, Nov. 2001, pp. 2997–3001.

- [19] S. Yang, A. Kavčić, and S. Tatikonda, "Feedback capacity of finite-state machine channels," *IEEE Trans. Inf. Theory*, vol. 51, no. 3, pp. 799–810, Mar. 2005.
- [20] P. O. Vontobel and D. M. Arnold, "An upper bound on the capacity of channels with memory and constraint input," in *Proc. IEEE Information Theory Workshop*, Cairns, Queensland, Australia, Sept. 2001, pp. 147–149.
- [21] J. Chen and P. H. Siegel, "Markov processes asymptotically achieve the capacity of finite-state intersymbol interference channels," *IEEE Trans. Inf. Theory*, vol. 54, no. 3, pp. 1295–1303, Mar. 2008.
- [22] T. S. Han and M. Sasaki, "Wiretap channels with causal state information: Strong secrecy," *IEEE Trans. Inf. Theory*, vol. 65, no. 10, pp. 6750–6765, Oct. 2019.
- [23] —, "Wiretap channels with causal state information: revisited," arXiv: 2001.03482, 2021.
- [24] B. Dai, C. Li, Y. Liang, Z. Ma, and S. Shamai Shitz, "Impact of action-dependent state and channel feedback on gaussian wiretap channels," *IEEE Trans. Inf. Theory*, vol. 66, no. 6, pp. 3435–3455, Jan. 2020.
- [25] B. Dai, Z. Ma, and Y. Luo, "Finite state Markov wiretap channel with delayed feedback," *IEEE Trans. Inf. Forensics Secur.*, vol. 12, no. 3, pp. 746–760, Mar. 2017.
- [26] S. Hanoglu, S. R. Aghdam, and T. M. Duman, "Artificial-noise-aided secure transmission over finite-input intersymbol interference channels," in *Proc. 25th Int. Conf. Telecommun.*, St. Malo, France, June 2018, pp. 346–350.
- [27] J. de Dieu Mutangana and R. Tandon, "Blind MIMO cooperative jamming: secrecy via ISI heterogeneity without CSIT," *IEEE Trans. Inf. Forensics Secur.*, vol. 15, pp. 447–461, June 2020.
- [28] Y. Sankarasubramaniam, A. Thangaraj, and K. Viswanathan, "Finite-state wiretap channels: Secrecy under memory constraints," in *Proc. IEEE Information Theory Workshop*, Taormina, Italy, Oct. 2009, pp. 115–119.
- [29] I. Csiszár and J. Körner, "Broadcast channels with confidential messages," *IEEE Trans. Inf. Theory*, vol. 24, no. 3, pp. 339–348, May 1978.
- [30] U. M. Maurer, "The strong secret key rate of discrete random triples," in *Communications and Cryptography: Two Sides of One Tapestry*, Norwell, MA, USA: Kluwer, 1994, pp. 271–285.
- [31] A. D. Wyner, "The wire-tap channel," *The Bell System Technical Journal*, vol. 54, no. 8, pp. 1355–1387, Oct. 1975.
- [32] M. Bloch and J. Barros, *Physical-layer security: from information theory to security engineering*, 1st ed. New York, NY, USA: Cambridge University Press, 2011.
- [33] M. R. Bloch and J. N. Laneman, "Strong secrecy from channel resolvability," *IEEE Trans. Inf. Theory*, vol. 59, no. 12, pp. 8077–8098, Dec. 2013.
- [34] M. Bellare, S. Tessaro, and A. Vardy, "Semantic security for the wiretap channel," in *Proc. CRYPTO 2012*, vol. 7417, Berlin, Heidelberg, 2012, pp. 294–311.
- [35] T. S. Han, *Information-Spectrum Methods in Information Theory*. Berlin, Heidelberg: Springer, 2003.
- [36] M. Bloch and J. N. Laneman, "On the secrecy capacity of arbitrary wiretap channels," in *Proc. 46th Annual Allerton Conf. Commun. Control and Computing*, Monticello, IL, USA, Sept. 2008, pp. 818–825.
- [37] D. M. Arnold, H.-A. Loeliger, P. O. Vontobel, A. Kavčić, and W. Zeng, "Simulation-based computation of information rates for channels with memory," *IEEE Trans. Inf. Theory*, vol. 52, no. 8, pp. 3498–3508, Aug. 2006.
- [38] P. Sadeghi, P. O. Vontobel, and R. Shams, "Optimization of information rate upper and lower bounds for channels with memory," *IEEE Trans. Inf. Theory*, vol. 55, no. 2, pp. 663–688, Feb. 2009.
- [39] A. Dempster, N. Laird, and D. Rubin, "Maximum likelihood from incomplete data via the EM algorithm," *Journal of the Royal Statistical Society. Series B (Methodological)*, pp. 1–38, 1977.
- [40] C. F. J. Wu, "On the convergence properties of the EM algorithm," *The Annals of Statistics*, vol. 11, no. 1, pp. 95–103, 1983.
- [41] W. Xiang and S. Pietrobon, "On the capacity and normalization of ISI channels," *IEEE Trans. Inf. Theory*, vol. 49, no. 9, pp. 2263–2268, Sept. 2003.
- [42] K. L. Judd, *Numerical Methods in Economics*. London: The MIT Press, 1998.